Distribution
Category UC-70

SAND85-0709
Unlimited Release
Printed August 1986

Effects of Sample Size on the Mechanical Behavior of Topopah Spring Tuff

R. H. Price
Geomechanics Division
Sandia National Laboratories
Albuquerque, New Mexico 87185

ABSTRACT

Thirty-four mechanical experiments were performed on intact cylindrical samples of the Topopah Spring Member of the Paintbrush Tuff taken from an outcrop on Busted Butte, southeast of Yucca Mountain in southern Nevada. The samples ranged in diameter from 25.4 to 228.6 mm, and all had a nominal length to diameter ratio of 2:1. All samples were water saturated and deformed in compression at atmospheric confining pressure, room temperature, and a nominal strain rate of 10^{-5} s^{-1}. Young's modulus and Poisson's ratio were found to have no significant trend with changes in sample size. Ultimate strength and axial strain at failure were both inversely related to sample diameter, with simple power-law models fitting the data trends very well.

Contents

INTRODUCTION

Yucca Mountain, located near the southwest margin of the Nevada Test Site (NTS) in southern Nevada, is being evaluated as a potential site for underground disposal of nuclear waste. Yucca Mountain primarily consists of layered volcanic tuff (Bish et al., 1981). At present, the Topopah Spring Member of the Paintbrush Tuff is being tested for physical, thermal, and mechanical properties as part of the Nevada Nuclear Waste Storage Investigations (NNWSI) Project, which is administered by the Nevada Operations Office of the U.S. Department of Energy (DOE).

This report is the seventh (see Olsson and Jones, 1980; Price, Nimick, and Zirzow, 1982; Price, Spence, and Jones, 1984; Price et al., 1985; Nimick et al., 1985; Nimick et al., in preparation) that presents data from mechanical tests conducted on intact samples of the Topopah Spring Member. The test specimens used in this study were obtained from an outcrop on the southeast flank of Busted Butte, and are from a section of the Topopah Spring Member approximately stratigraphically equivalent to the proposed repository horizon within Yucca Mountain. The mechanical property data contained in this report ultimately will be used to aid in assessing the mineability and stability of underground openings in the Topopah Spring Member, and to evaluate predicted near- and far-field responses to the presence of a repository within the unit. This test series was designed to study the effects of changes in sample size by deforming water-saturated samples ranging in diameter from 25.4 to 228.6 mm under atmospheric pressure, room temperature, and constant strain rate (10^{-5} s^{-1}) conditions.

Figure 1 shows the locations of the NTS, Yucca Mountain, and Busted Butte, and Figure 2 shows the stratigraphic setting of the Topopah Spring Member. All symbols and abbreviations used in this report can be found in Table 1. Within this table the terms are defined, conventions explained, and standard units assigned. The sample/test identification used throughout this report consists of three to five numbers and letters.

EXPERIMENTAL TECHNIQUES

Test Apparatus and Techniques

The mechanical experiments were performed on a load frame with a maximum load capacity of 5.0 MN. A constant displacement rate of the loading piston was achieved by servo-control of the hydraulic loading ram while monitoring a linear variable displacement transformer (LVDT) at the base of the loading column.

Throughout this test series, axial stress (σ_{az}) was calculated by dividing the force, measured on a standard load cell, by the original cross-sectional area of the sample. Axial strain (ε_{az}) was calculated by one of four methods, either 1. averaging the measured displacements on two diametrically opposed LVDTs mounted directly on the sample and dividing by the average value of the original gage lengths, 2. dividing the measured displacement on the LVDT mounted between the lower end-cap and the lower base plate (minus machine and end-cap displacements) by the original sample length, 3. dividing the measured displacement on the LVDT mounted between the upper and lower end-caps (minus end-cap displacements) by the original sample length, or 4. dividing the measured displacement on the LVDT mounted between two aluminum mounts epoxied directly onto the sample (each mount was located approximately one-third of the sample length from the sample end) by the original gage length. Lateral (transverse) displacement was measured across one sample diameter (located in the middle of the sample) or two sample diameters (located at 40% of the sample length from each end) by one or two ring gage(s) (as described by Holcomb and McNamee, 1984). Lateral strain (ε_{lat}) was then obtained by dividing the lateral displacement by the original diameter of the test specimen. Axial force, axial displacement, transverse displacement, and time data were collected and reduced on a *DEC* (*Digital Equipment Corporation*) LSI 11/23 computer, with software described by Holcomb and Jones (1983). The data were subsequently transferred to a *DEC* VAX 11/780 for plotting, using GRAPH II (Selleck, 1984), and analysis.

Calibrations

The calibration data for the load cell, axial displacement gages, lateral displacement gages, and test system calibration checks, as well as a discussion of that data, are presented in Appendix A.

Sample Preparation

Rocks for this study were collected as large (up to 3 m^3), irregular blocks from an outcrop on the southeastern flank of Busted Butte, in the southwest corner of the NTS, just east of the southern end of Yucca Mountain (Figure 1). The outcrop is located very close to north latitude 36°46′19″, west longitude 116°25′28″. Figure 3 summarizes a measured section of the tuff exposures at the sample location.

Cylindrical samples with diameters slightly greater than the final dimensions were cored from the large blocks. These samples were then cut and machined to right-circular cylinders with tolerances of ±0.25 mm on the diameter and ±2.0 mm on the length.

The samples had nominal finished diameters of 25.4, 50.8, 82.6, 127.0, and 228.6 mm, and in all cases a 2:1 length to diameter ratio was maintained. Pieces cut from the sample ends were used in mineralogy and bulk property studies (reported by Price et al., in preparation), and the finished cylinders were the mechanical test specimens.

Macroscopically, samples from the welded, devitrified zone consist of two main components. The majority of the rock consists of a fine-grained matrix identifiable by its dark, generally purple or reddish-brown color. Gray regions of vapor-phase-altered material vary in size and are quite common. (For a detailed discussion of the petrology of these rocks, see Price et al., in preparation) In addition to these petrologic regions, many of the samples contain small (open and closed) lithophysae (see Price et al., 1985) and "healed" fractures. All of the rock specimens were described by F. B. Nimick prior to mechanical testing. These brief descriptions are presented in Table 2.

All samples were stored in distilled water and/or groundwater from Well J-13 (NTS). Before testing, the samples were submerged and subjected to 3 or more vacuum saturation cycles that included at least 18 hours under an active vacuum and 6 hours at ambient pressure. The samples were considered to be saturated when the weight gain after a given saturation step was less than or equal to 0.05% of the weight at the beginning of the step.

After saturation, each sample was placed between steel end pieces (i.e. end-caps), the axial and transverse transducers mounted, the sample assembly placed between the loading ram and the load cell, and the test begun.

Test Conditions

The experiments presented in this report were actually run in two separate series, approximately one year apart. During both test series, experiments were performed on samples with diameters of 25.4, 50.8, 82.6, and 127.0 mm. The only two 228.6 mm samples were tested during the second series. The samples for each test series were obtained from different blocks, but all the blocks were taken from the same outcrop on Busted Butte. The two series are denoted as 1 and 2 (signifying chronological order) in Table 3 and in Appendix A. Since the samples were from the same location, the calibration procedures used were identical, and the testing apparatus and procedures were the same, the mechanical results are all treated as a single, larger group of data.

All samples were deformed in compression under saturated, drained, unconfined, room temperature, and constant strain rate (10^{-5} s^{-1}) conditions.

EXPERIMENTAL RESULTS

General

A summary of the mechanical property results is given in Table 3. In addition, the means, standard deviations, and ranges of Young's moduli, Poisson's ratios, ultimate strengths, and axial strains at failure for each sample size are summarized in Table 4.

The differential stress/axial strain curves are presented in Figures 4-8. The general shapes of the stress/strain curves for the densely welded, devitrified samples are very similar to results reported for previous tests on other densely welded, silicic tuff from the Topopah Spring Member (e.g., Price, Spence, and Jones, 1984; Nimick, et al., 1985).

Discussion

Elastic Properties: Young's modulus (E) and Poisson's ratio (ν) were calculated from the axial stress, axial strain, and lateral strain data for each test. In all cases, the data considered in these calculations were taken in the range of stresses from 10 to 50% of the ultimate sample strength.

Plots of the mean plus or minus one standard deviation of Young's modulus versus sample diameter and of Poisson's ratio versus sample diameter are presented in Figures 9 and 10, respectively. Neither of these graphs reveal a distinct trend in elastic properties with changing sample size, a result which was not surprising (see Lama and Vutukuri, 1978, p. 62).

Failure Strength: Experimental investigations on rocks deformed in compression have produced a range of strength/sample size relationships. Trends in strength change with increasing sample size include 1. increasing (e.g., Crane, 1926; Hoskins and Horino, 1969), 2. decreasing (e.g., Abou-Sayed and Brechtel, 1976; Bieniawski, 1968; Einstein, Baecher, and Hirschfeld, 1970; Hoskins and Horino, 1969; Košťák and Bielenstein, 1971; Lundborg, 1967; Mogi, 1962; Pratt, et al., 1972), 3. initial increasing, followed by decreasing (e.g., Alekseev, et al., 1970; Hoskins and Horino, 1969), and 4. no change (e.g., Hodgson and Cook, 1970; Obert, Windes, and Duvall, 1946; Swolfs, 1983). These various behaviors are the result of many factors, including rock type (i.e., porosity, grain size, inhomogeneity size, isotropy, etc.), range of sample sizes tested, sample shape, sample length to width ratio, and test conditions. However, a majority of the previous experimental studies have indicated an inverse strength/size relationship, and this trend was found to be true in this investigation.

In many of the cases where strength and sample size were inversely related, the strength decrease was fit well with a simple power-law model. Figure 11 shows a plot of the strength data with a power-law, best fit. The resulting fit is as follows:

$$\sigma_u = 1944.\ D^{-0.846} + 69.5, \tag{1}$$

where σ_u is ultimate strength (MPa) and D is sample diameter (mm). The asymptotic stress term (69.5 Mpa) was determined in an iterative process by subtracting stress from all σ_u values, making least-squares fits in log-log space, changing the subtracted stress value, and maximizing the linear correlation coefficient from the log-log fits.

Failure Strain: A plot of axial strain at failure versus sample diameter reveals a similar trend (Figure 12). The resulting power-law, best fit is as follows:

$$(\varepsilon_{az})_u = 11.6\ D^{-0.268}, \tag{2}$$

where $(\varepsilon_{az})_u$ is axial strain at ultimate strength (millistrains) and D is sample diameter (mm). This result is to be expected since the welded Topopah Spring Member, under these conditions, is essentially linear elastic up to failure and we observe no effect of sample size on Young's modulus (Figure 9).

SUMMARY

Thirty-four uniaxial compression experiments were performed on intact cylindrical samples of the Topopah Spring Member of the Paintbrush Tuff. Sample diameters ranged from 25.4 to 228.6 mm, in order to study the effects of sample size on mechanical properties. All of the experiments were performed on water-saturated samples at room temperature and a nominal strain rate of 10^{-5} s^{-1}. Results show Young's modulus and Poisson's ratio to be essentially independent of sample size, and ultimate strength and axial strain at failure to be inversely related to sample diameter. Simple power-law models fit the strength and strain data trends very well.

Acknowledgements: The author would like to express his great appreciation for the work of M. E. Stavig and S. J. Spence, who measured, saturated, and tested the samples. Thanks also to F. B. Nimick for his careful sample descriptions.

REFERENCES

Abou-Sayed, A. S., and Brechtel, C. E.
Experimental Investigation of the Effects of Size on the Uniaxial Compressive Strength of Cedar City Quartz Diorite, Proc. 17th Symposium on Rock Mechanics, Snowbird, Utah, 1976, p. 5D6,1-9.

Alekseev, A. D., Zhuravlev, V. I., Yarovaya, L. I., and Molchanenko, V. S.
Effect of the Geometryand Fracturing of Rock Specimens on Their Strength, Sov. Min. Sci., No. 3, May-June, 1970, pp. 281-285.

Bieniawski, Z. T.
The Effect of Specimen Size on Compressive Strength of Coal, Int. J. Rock Mech. Min. Sci., Vol. 5, 1968, pp. 325-335.

Bish, D. L., Caporuscio, F. A., Copp, J. F., Crowe, B. M., Purson, J. D., Smyth, J. R., and Warren, R. G.
Preliminary Stratigraphic and Petrologic Characterization of Core Samples from USW-G1, Yucca Mountain, Nevada, Los Alamos National Laboratory Report, LA-8840-MS, Los Alamos, NM, 1981.

Crane, W. R.
Strength of Ore and Top Rock in the Red Iron-Ore Mines of the Birmingham District, Alabama, U. S. Bur. Min. Tech. Pap. 379, 1926.

Einstein, H. H., Baecher, G. B., and Hirschfeld, R. C.
The Effect of Size on the Strength of a Brittle Rock, Proceedings of the 2nd Cong. Int. Soc. Rock Mech., Belgrade, 1970, Vol. 2, pp. 7-13.

Hodgson, K., and Cook, N. G. W.
The Effects of Size and Stress Gradient on the Strength of Rock, Proceedings of the 2nd Cong. Int. Soc. Rock Mech., Belgrade, 1970, Vol. 2, pp. 31-34.

Holcomb, D. J., and Jones, A. K.
Data Acquisition for the Rock Mechanics Lab, Sandia National Laboratories Report, SAND83-0646, Albuquerque, NM, August 1983.

Holcomb, D. J., and McNamee, M. J.
Displacement Gage for the Rock Mechanics Laboratory, Sandia National Laboratories Report, SAND84-0651, Albuquerque, NM, December 1984.

Hoskins, J. R. and Horino, F. G.
Influence of Spherical Head Size and Specimen Diameters on the Uniaxial Compressive Strength of Rocks, U. S. Bur. Min. Invest. 7234, 1969, 16 p.

Košťák, B. and Bielenstein, H. U.
Strength Distribution in Hard Rock, Int. J. Rock Mech. Min. Sci., Vol. 8, 1971, pp. 501-521.

Lama, R. D., and Vutukuri, V. S.
Handbook on Mechanical Properties of Rocks - Testing Techniques and Results - Volume II, Series on Rock and Soil Mechanics, Vol. 3 (1978), No. 1, Trans Tech Publications, Clausthal, Germany, 1978, p. 62.

Lundborg, N.
The Strength-Size Relation of Granite, Int. J. Rock Mech. Min. Sci., Vol. 4, 1967, pp. 269-272.

McNamee, M. J.
A Calibrator for Displacement Gages Used in the Rock Mechanics Laboratory, Sandia National Laboratories Report, SAND85-0548, Albuquerque, NM, May 1985.

Mogi, K.
The Influence of the Dimensions of Specimens on the Fracture Strength of Rocks, Bull. Earthquake Res. Inst., Tokyo Univ., Vol. 40, 1962, pp. 155-170.

Nimick, F. B., Price, R. H., Van Buskirk, R. G. and Goodell, J. R.
Uniaxial and Triaxial Compression Test Series on Topopah Spring Tuff from USW G-4, Yucca Mountain, Nevada, Sandia National Laboratories Report, SAND84-1101, Albuquerque, NM, December 1985.

Nimick, F. B., Van Buskirk, R. G. and MacFarland, A. J.
Uniaxial and Triaxial Compression Test Series on Topopah Spring Member from USW G-2, Yucca Mountain, Nevada, Sandia National Laboratories Report, SAND85-0703, Albuquerque, NM, in preparation.

Obert, L., Windes, S. L., and Duvall, W. I.
Standardized Tests for Determining the Physical Properties of Mine Rock, U. S. Bur. Min. Invest. 3891, 1946.

Olsson, W. A. and Jones, A. K.
Rock Mechanics Properties of Volcanic Tuffs from the Nevada Test Site, Sandia National Laboratories Report, SAND80-1453, Albuquerque, NM, November 1980.

Pratt, H. R., Black, A. D., Brown, W. S., and Brace, W. F.
The Effect of Specimen Size on the Mechanical Properties of Unjointed Diorite, Int. J. Rock Mech. Min. Sci., Vol. 9, 1972, pp. 513-529.

Price, R. H.
Analysis of Rock Mechanics Properties of Volcanic Tuff Units from Yucca Mountain, Nevada Test Site, Sandia National Laboratories Report, SAND82-1315, Albuquerque, NM, August 1983.

Price, R. H., Connolly, J. R., and Keil, K.
Analysis of the Effects of Changes in Environmental Conditions on the Mechanical Properties of the Welded, Devitrified Topopah Spring Member of the Paintbrush Tuff Sandia National Laboratories Report, SAND86-1131, Albuquerque, NM, in preparation.

Price, R. H., Nimick, F. B., Connolly, J. R., Keil, K., Schwartz, B. M., and Spence, S. J.
Preliminary Characterization of the Petrologic, Bulk, and Mechanical Properties of a Lithophysal Zone Within the Topopah Spring Member of the Paintbrush Tuff, Sandia National Laboratories Report, SAND84-0860, Albuquerque, NM, February 1985.

Price, R. H., Nimick, K. G., and Zirzow, J. A.
Uniaxial and Triaxial Compression Test Series on Topopah Spring Tuff, Sandia National Laboratories Report, SAND82-1723, Albuquerque, NM, October 1982.

Price, R. H., Spence, S. J., and Jones, A. K.
Uniaxial and Triaxial Compression Test Series on Topopah Spring Tuff From USW GU-3, Yucca Mountain, Southern Nevada, Sandia National Laboratories Report, SAND83-1646, Albuquerque. NM, February 1984.

Selleck, C. B.
GRAPH II: A Digitizing and Graph Plotting Program, Sandia National Laboratories Report, SAND84-0302, Albuquerque, NM, March 1984.

Stavig, M. E., and Price, R. H.
A Study of the End Effects on Samples in the Rock Mechanics Laboratory, Sandia National Laboratories Report, SAND86-1132, Albuquerque, NM, in preparation.

Swolfs, H. S.
Aspects of the Size-Strength Relationship of Unjointed Rocks, in Proceedings of the 24^{th} U. S. Symposium on Rock Mechanics: Rock Mechanics, Theory - Experiment - Practice, C. C. Mathewson (Ed.), 1983, pp. 501-510.

Table 1.
Symbols, Abbreviations, Definitions, Conventions and Units

SYMBOL	DEFINITION	UNITS
E	Elastic constant : Young's modulus	GPa
ν	Elastic constant : Poisson's ratio	—
σ_1 , σ_2 , σ_3	Principal stresses, compressive stresses are positive	MPa
σ_{az}	Stress parallel to the sample axis, ($\sigma_{az} \approx \sigma_1$)	MPa
$(\sigma_{az})_u$	Ultimate axial stress	MPa
ε_1 , ε_2 , ε_3	Principal strains, compressive strains are positive	—
ε_{az}	Strain parallel to the sample axis ($\varepsilon_{az} \approx \varepsilon_1$)	—
ε_{lat}	Strain perpendicular to the sample axis ($\varepsilon_{lat} \approx \varepsilon_2 \approx \varepsilon_3$)	—
$(\varepsilon_{az})_u$	Axial strain at ultimate axial stress	
f	Force f_a : actual force f_m : measured force	N
δ	Displacement δ_a : actual displacement δ_m : measured displacement	m
R^2	Linear correlation coefficient	—
e_m	Error of the measured value (e.g., $100 \times \frac{f_m - f_a}{f_a}$)	%

ABBREVIATION	DEFINITION
NTS	Nevada Test Site
NNWSI	Nevada Nuclear Waste Storage Investigations
DOE	Department of Energy
J-13	Drillhole east of Yucca Mountain
USBS	United States Bureau of Standards
LVDT	Linear variable displacement transformer

Table 2a.
Brief Descriptions of the 25.4 mm Samples

Sample ID	Description (from F. B. Nimick, personal communication)
12A2	Densely welded; chocolate; very few pumice fragments, one on an end.
12A3	Densely welded; chocolate; 10% pumice fragments surrounded by thin light brown envelopes; some larger light brown particles (also pumice?) intersecting both ends, some pumice elongated, but no consistent orientation.
13A2	Densely welded; chocolate; 50 mm long pink-orange lithic; otherwise 20% randomly scattered pumice(?) surrounded by thin envelopes of alteration.
26C1	Densely welded; red-brown; irregular dark brown areas; several small lithics including one on an end (corner); minor light-colored, altered areas.
26D1	Densely welded; muddy brown and pink-brown areas; pink altered halos around pumice/lithic inclusions, one of which intersects end (corner); one healed, discontinuous fracture (~25 mm long) 60-70° to core axis; one healed discontinuous fracture (~20 mm long) 90° to core axis; sides not smooth.
26E1	Densely welded; sub-equal red-brown and muddy-brown matrix; one large (25×12 mm) inclusion (calcite? opal?); possible fabric at 10-20° to core axis; one end chipped.

Table 2b.
Brief Descriptions of the 50.8 mm Samples

Sample ID	Description (from F. B. Nimick, personal communication)
10X12	Densely welded; chocolate; minor pumice; one open lithophysa, near middle, partly filled with calcite.
10Y47	Densely welded; chocolate; 10% pumice; one lithophysa ~15 mm from end, mostly filled.
10Z15	Densely welded; chocolate; large (~30 mm) gray area at one end; several small, healed fractures occur at both ends; one mostly filled lithophysa.
26A1	Densely welded; pink-brown to muddy brown; one large (25×38 mm) pink area; two healed fractures ~30° to sample axis and ~60° to each other, both intersect ends, first fracture has white filling, second is brown w/gray halo; possible fabric at 10-20° to sample axis.
26B1	Densely welded; red-brown, some gray-brown patches; some pumice, one large fragment (25×19 mm); one healed fracture across one end 60° to sample axis, white filling w/gray halo, several other discontinuous healed fractures; one flattened lithophysa intersects opposite end from fracture; some inclusions with pink alteration halos.
28A2	Densely welded; pink-brown to muddy-brown; one open lithophysa extends 65 mm from an end at ~10° to sample axis, opening 0 to 8 mm, partially filled with calcite(?), gray alteration halo, closed extension of lithophysa extends within 15 mm of other end of sample; two healed fractures radiate from open lithophysa for 90 mm at 0-30° to sample axis and at 20-45° to each other, a third open fracture extends from open lithophysa at 30-40° to sample axis.

Table 2c.
Brief Descriptions of the 82.6 mm Samples

Sample ID	Description (from F. B. Nimick, personal communication)
10E3	Densely welded; light brown to chocolate; 5% lithics/pumice; one medium grey patch; 9 healed fractures ~80-90° to core axis.
10E4	Densely welded; chocolate; one large discontinuous fracture and several short fractures/foliation, all ~80° to core axis.
11A1	Densely welded; chocolate to light brown; 5% lithics/pumice; one continuous fracture, two discontinuous fractures, and many smaller cracks, all healed.
11A2	Densely welded; chocolate with light brown patch; 5% lithics/pumice; one large grey-brown patch with 50 mm filled lithophysa; one healed fracture continuous end to end.
11C1	Densely welded; chocolate; two large (~65 mm) grey patches; ~35 mm lithic near end; one continuous fracture at end and three discontinuous fractures near center of sample.
11D1	Densely welded; brown; 5% lithics/pumice; several minor fractures.
211	Densely welded; two bands of color, purple- and pink-brown; most lithics have alteration halos; 4 discontinuous healed fractures at 0-45° to axis, all intersect an end and have gray halos.
231	Densely welded; pink-brown; most lithics have pink alteration halos; one continuous fracture, several long (38-127 mm) healed discontinuous fractures with gray halos, and the rock fabric is ~45° to axis.
271	Densely welded; pink- with purple-brown; 3 open flattened lithophysae, one near end is 100 mm long open up to 8 mm with some calcite fill, one is 37 mm long, open up to 3 mm, and third is 25 mm long, mostly filled w/ calcite; one healed fracture extending from an end at 40-50° to sample axis, several other healed, discontinuous fractures.

Table 2d.
Brief Descriptions of the 127.0 mm Samples

Sample ID	Description (from F. B. Nimick, personal communication)
10A1	Densely welded; chocolate, some light brown; five partially filled lithophysal slits (25-75 mm long); minor short fractures.
10A2	Densely welded; chocolate, some light brown; one long (~90 mm) lithophysal slit (25 mm filled, 65 mm open); minor small fractures.
10C1	Densely welded; chocolate to light brown; some pumice; one partially filled lithophysal slit (50 mm), one 75 mm slit completely filled; 10-15 discontinuous fractures at ~90° to axis.
10C2	Densely welded; light brown to chocolate; several small lithics with alteration halos; one axial fracture with alteration fringe, 10-15 minor fractures.
10D1	Densely welded; chocolate to light brown; 65 mm lithic with 25 mm fringe; three partially filled lithophysal slits (25-75 mm); many small fractures.
10D2	Densely welded; light brown to chocolate; six flattened lithophysae (five filled); one axial fracture with alteration fringe, many short fractures.
221	Densely welded; pink-brown; some lithics (up to 37 mm) with pink alteration halos; three partially open lithophysae, one extends from end 64 mm, open up to 8 mm, second 64-76 mm open at most 6 mm (both at 0° to axis), third 37 mm open 3 mm, at 30°; fractures/fabric parallel to axis.
234	Densely welded; pink- to muddy- brown; alteration halos around lithics; one healed fracture across entire sample at 80-90° to axis, with symmetrical halos of gray, white, and brown alteration.
261	Densely welded; pink-brown; lithics with pink alteration halos; one open lithophysa extending 12 mm from end, open up to 3 mm; numerous healed discontinuous fractures, most at 10-30° to axis.
281	Densely welded; purple-brown; large (19 by 50 mm) lithic; four partly filled, but open (up to 19 mm) lithophysae, two are connected by a fracture, one 165 mm is 0-40° to axis, second is 115 mm at 0-20°, others are smaller, mostly filled; minor discontinuous healed fractures.
282	Densely welded; purple-brown; several small partly filled lithophysae; large healed fracture at 30° to axis, pink-brown halo, offsets fractures and lithophysae up to 13 mm.

Table 2e.
Brief Descriptions of the 228.6 mm Samples

Sample ID	Description (from F. B. Nimick, personal communication)
222	Densely welded; pink-brown; open lithophysa ~100 mm long at 0-20° to axis, partly filled, but open up to 8 mm, large alteration halo; one healed fracture 50 mm long at ~30° to axis, gray halo; another fracture from corner at ~45° to axis 300-330 mm long, offset 12 mm by first fracture (intersection angle ~30°), filled, many other less continuous healed fractures throughout sample, most are subparallel to axis.
283	Densely welded; purple-brown; many lithics have pink alteration halos; open lithophysa intersects end, opening 12 mm, 75% filled, sample chipped at lithophysa, 3 smaller open lithophysae; one healed fracture along entire length at 30° to axis, gray halo, offsets many smaller discontinuous healed fractures.

Table 3.
Summary Test Results

Series	Sample ID	Diameter (mm)	E (GPa)	ν	$(\sigma_{az})_u$ (MPa)	$(\varepsilon_{az})_u$ (milli)
1	12A2	25.4	45.8	0.22	203.2	4.8
1	12A3	25.4	44.2	0.21	132.2	3.3
1	13A2	25.4	34.9	0.21	113.3	4.7
2	26C1	25.4	47.3	0.19	274.3	5.9
2	26D1	25.4	42.5	0.14	198.6	5.0
2	26E1	25.4	47.2	0.19	241.3	5.5
1	10X12	50.8	34.6	0.21	126.8	4.3
1	10Y47	50.8	35.9	0.20	143.2	4.3
1	10Z15	50.8	37.4	0.20	158.4	4.4
2	26A1	50.8	45.7	0.20	200.5	4.8
2	26B1	50.8	34.6	0.21	111.7	3.2
2	28A2	50.8	34.6	0.20	104.3	3.4
1	10E3	82.6	43.9	0.23	141.7	3.9
1	10E4	82.6	38.8	0.19	99.76	2.9
1	11A1	82.6	44.5	0.25	130.6	3.3
1	11A2	82.6	37.6	0.22	87.69	3.2
1	11C1	82.6	46.0	0.24	124.3	3.2
1	11D1	82.6	44.0	0.22	131.8	3.7
2	211	82.6	43.8	0.22	160.7	3.9
2	231	82.6	42.9	0.23	140.7	3.5
2	271	82.6	32.3	0.21	58.86	3.9
1	10A1	127.0	25.3	-	59.91	2.7
1	10A2	127.0	32.1	0.18	84.25	3.0
1	10C1	127.0	35.7	0.18	92.40	3.6
1	10C2	127.0	36.3	0.20	98.16	3.5
1	10D1	127.0	33.0	0.22	89.77	3.0
1	10D2	127.0	31.6	0.17	69.67	3.0
2	221	127.0	41.2	-	134.3	3.6
2	234	127.0	39.8	0.25	85.84	2.5
2	261	127.0	45.1	0.20	170.8	4.1
2	281	127.0	30.6	0.27	90.41	3.6
2	282	127.0	37.7	0.21	98.81	3.5
2	222	228.6	37.4	0.22	86.92	2.9
2	282	228.6	42.1	0.21	93.36	2.4

Table 4.
Statistical Summary of Mechanical Property Data

Diameter (mm)	E (GPa)	ν	$(\sigma_{az})_u$ (MPa)	$(\epsilon_{az})_u$ (milli)
25.4	43.7 ± 4.7	0.19 ± 0.03	193.8 ± 61.8	4.9 ± 0.9
50.8	37.1 ± 4.3	0.21 ± 0.01	140.8 ± 35.4	4.1 ± 0.6
82.6	41.5 ± 4.4	0.22 ± 0.02	119.6 ± 31.7	3.5 ± 0.4
127.0	35.3 ± 5.6	0.21 ± 0.03	97.7 ± 30.6	3.3 ± 0.5
228.6	39.7 ± 3.3	0.21 ± 0.00	90.1 ± 4.6	2.7 ± 0.4

Each value is the mean ± one standard deviation.

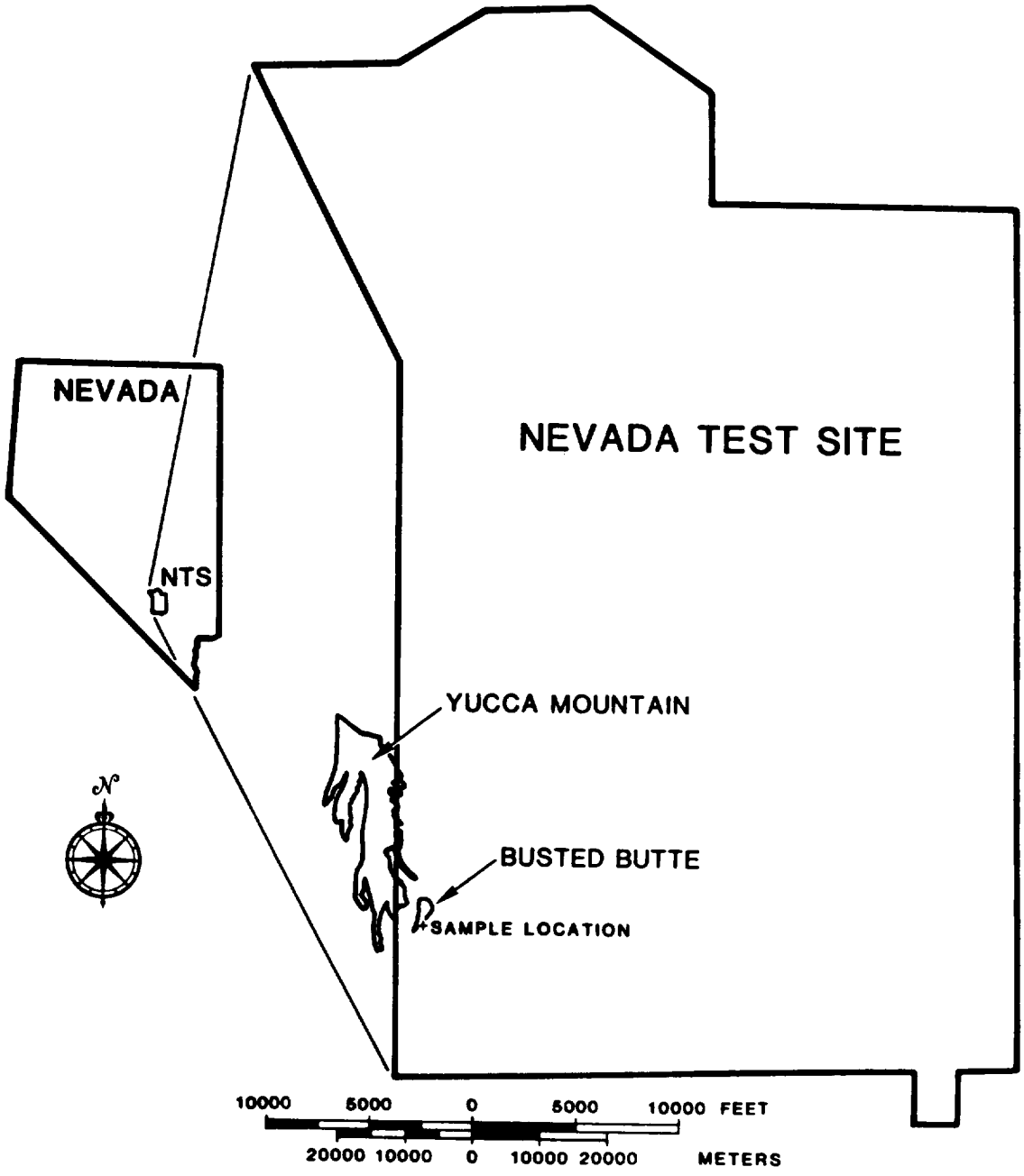

Figure 1.
Location Map of the Nevada Test Site, Yucca Mountain, and Busted Butte

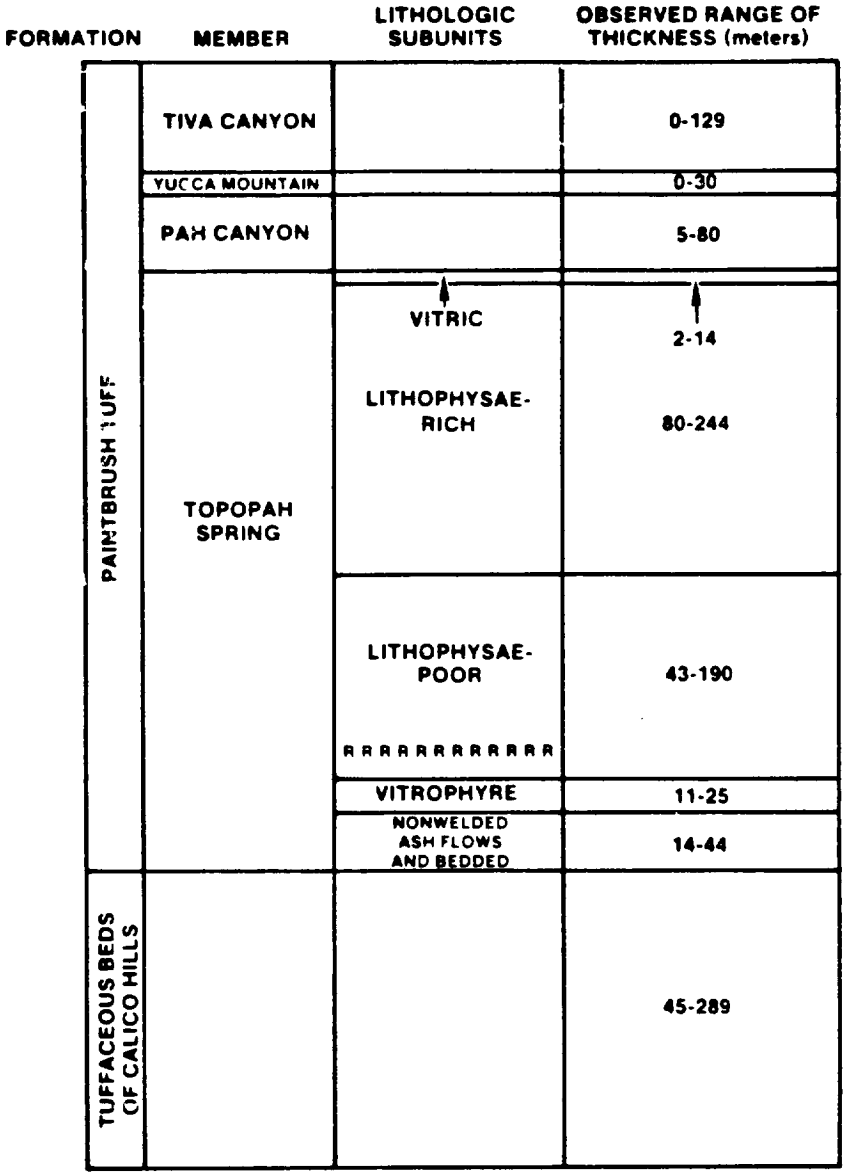

Figure 2.
Yucca Mountain Stratigraphic Column

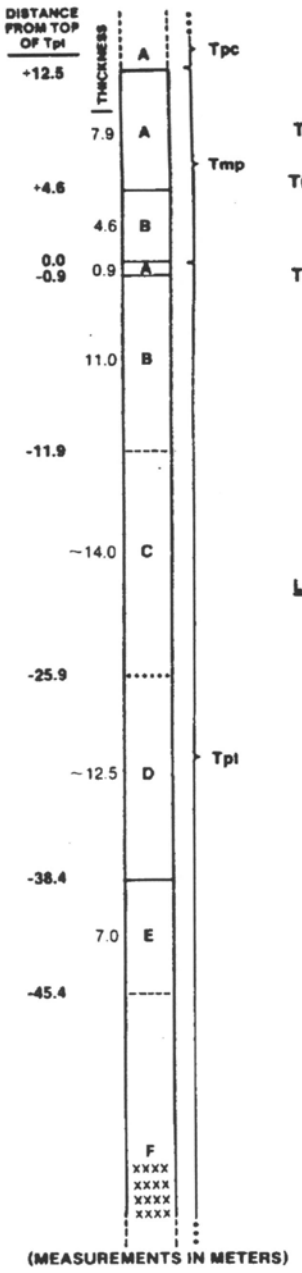

LITHOLOGY

Tpc - A: DENSELY WELDED TUFF, MODERATE LEDGEFORMER, ABUNDANT VERTICAL FRACTURES.

Tmp - A: BEDDED TUFF, BUFF-GRAY TO PALE ORANGE BROWN, PUMICE-RICH.
B: NONWELDED TUFF, REDDISH BROWN, RARE LITHOPHYSAE.

Tpt - A: VITROPHYRE, NON- TO MODERATELY WELDED, DARK GRAY TO BLACK, FRAGMENTAL TEXTURE.
B: MODERATELY TO DENSELY WELDED TUFF, REDDISH BROWN, RARE LITHOPHYSAE.
C: MODERATELY TO DENSELY WELDED TUFF, LIGHT GRAY, SPARSE BUFF-COLORED LITHIC INCLUSIONS, RARE LITHOPHYSAE.
D: MODERATELY TO DENSELY WELDED TUFF, PALE REDDISH BROWN, OCCASIONAL LITHOPHYSAE.
E: DENSELY WELDED TUFF, GRAY TO PALE REDDISH BROWN, ABUNDANT LITHOPHYSAE.
F: DENSELY WELDED TUFF, REDDISH BROWN TO GRAY, RARE LITHOPHYSAE.

LEGEND

—— WELL DEFINED CONTACT
---- APPROXIMATE CONTACT
••••• GRADATIONAL CONTACT
xxxx SAMPLED HORIZON

Tpc = TIVA CANYON MEMBER OF THE PAINTBRUSH TUFF
Tmp = INTERLAYERED BEDDED PAINTBRUSH TUFF
Tpt = TOPOPAH SPRING MEMBER OF THE PAINTBRUSH TUFF

Figure 3.
Measured Section from the Southeast Flank of Busted Butte

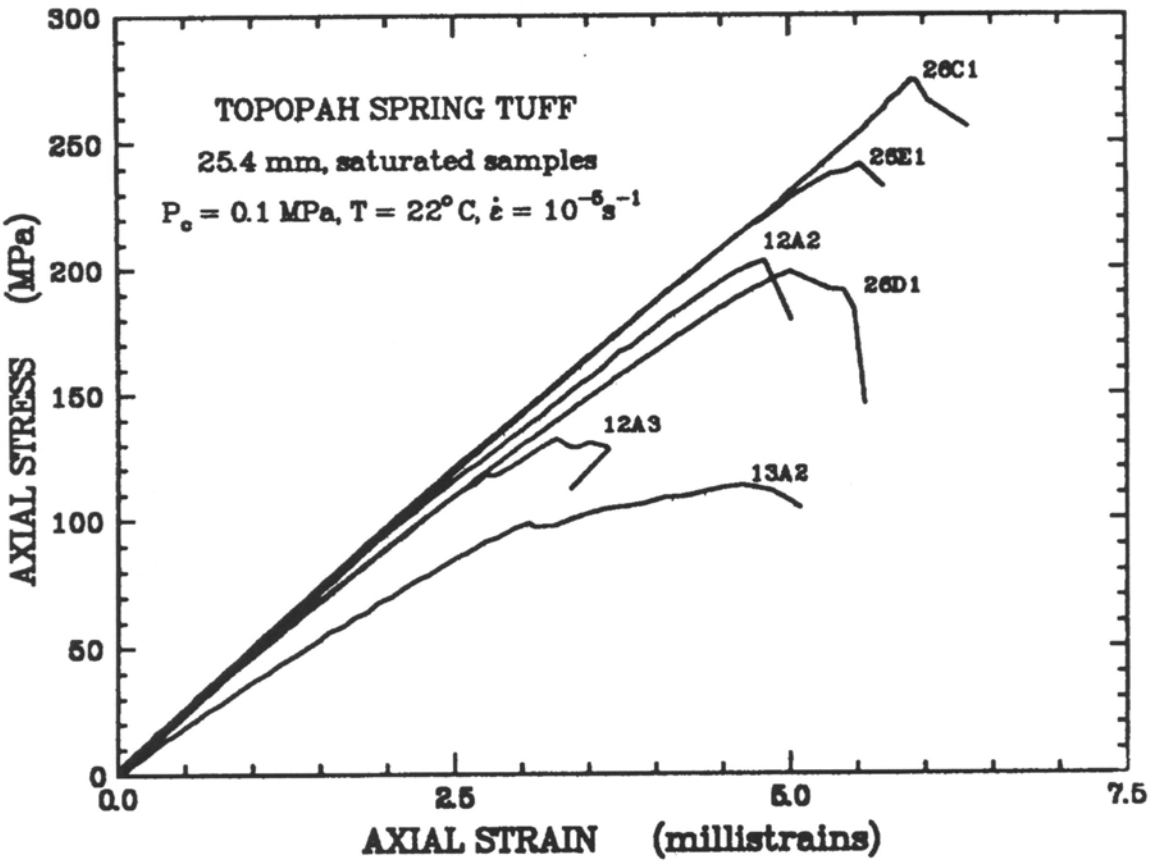

Figure 4.
Plots of Axial Stress Versus Axial Strain for All 25.4mm Samples

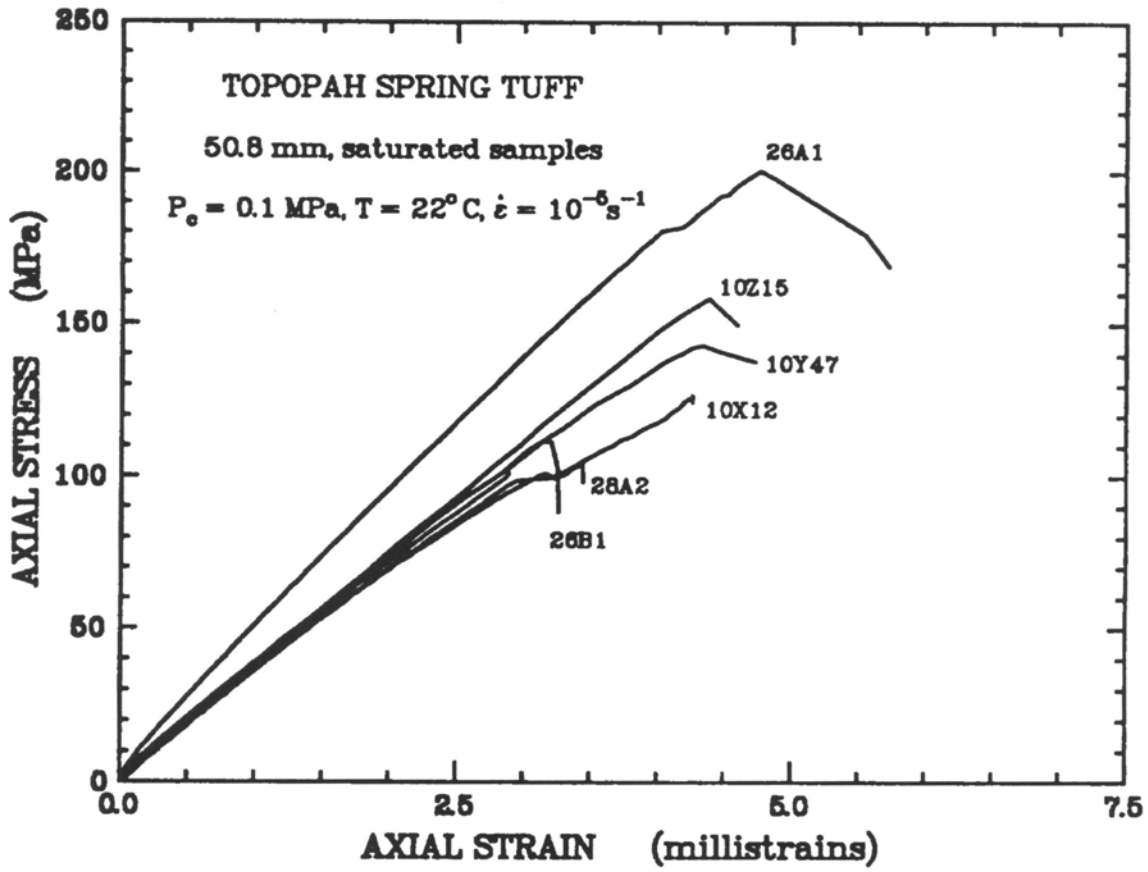

Figure 5.
Plots of Axial Stress Versus Axial Strain for All 50.8mm Samples

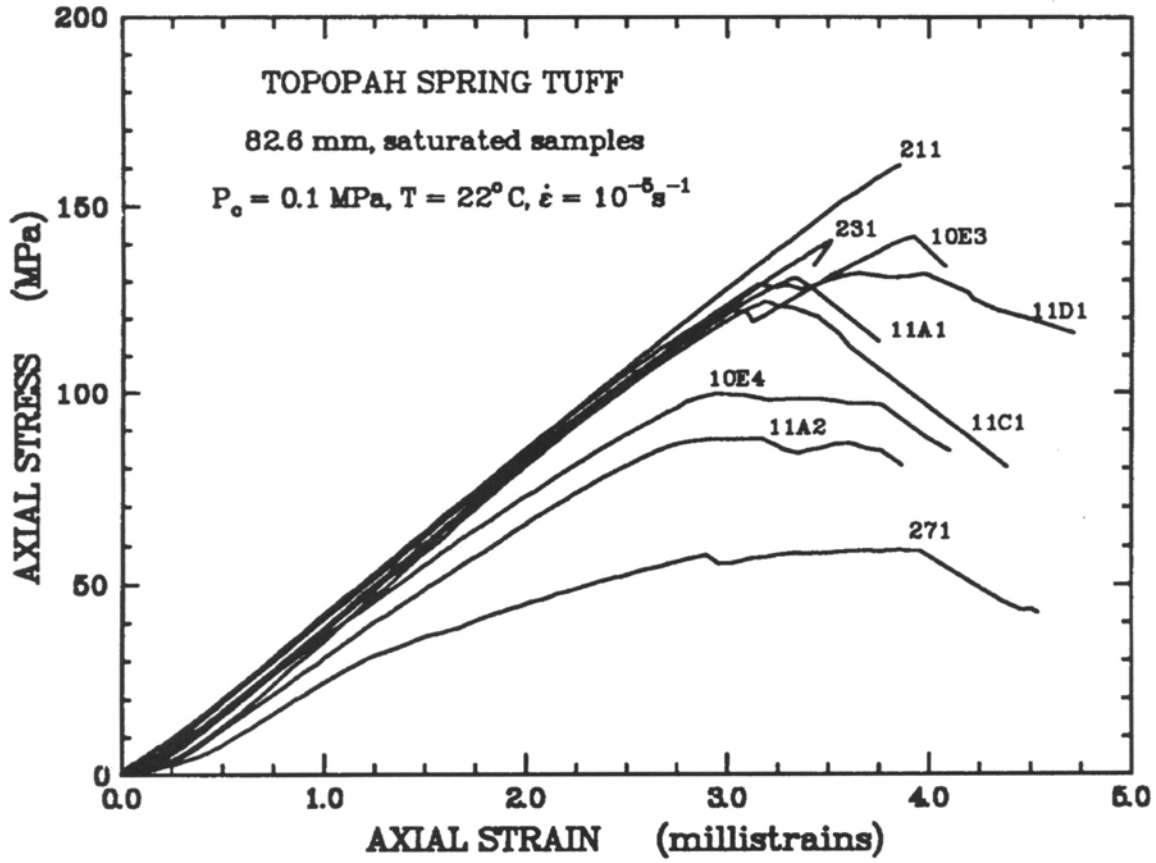

Figure 6.
Plots of Axial Stress Versus Axial Strain for All 82.6mm Samples

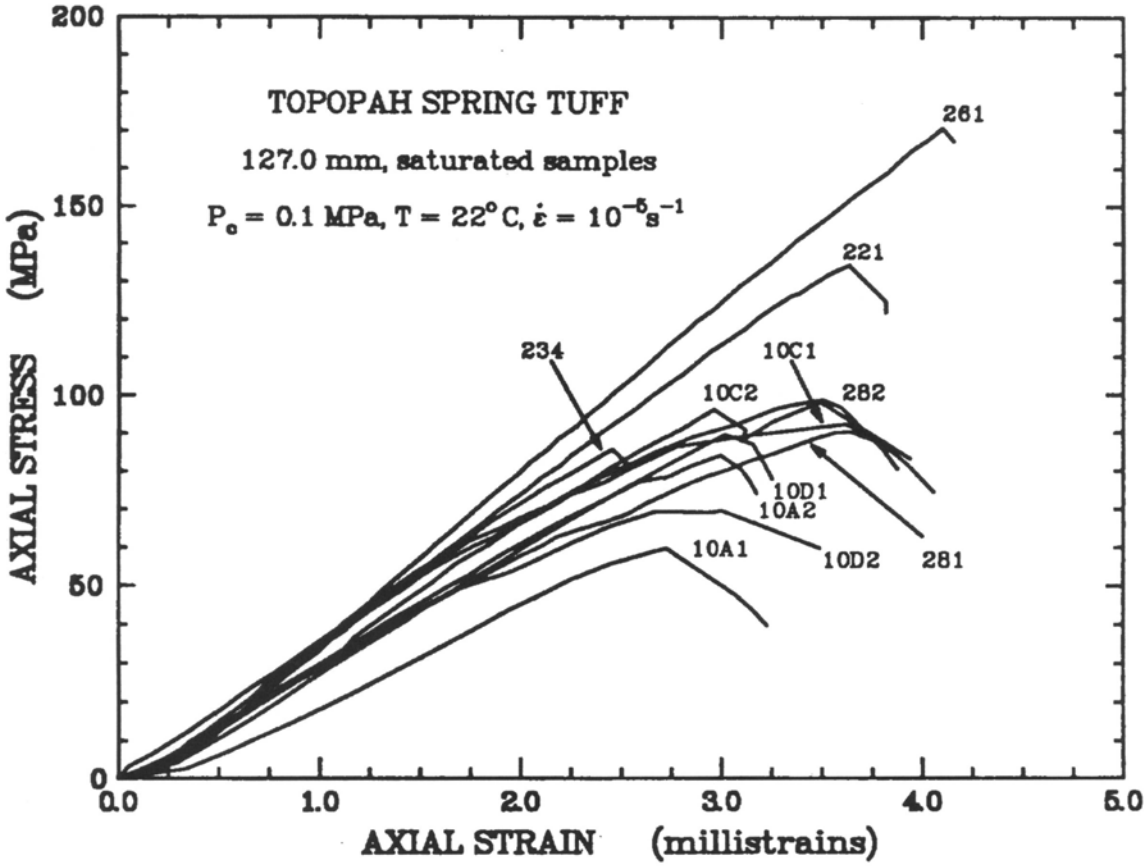

Figure 7.
Plots of Axial Stress Versus Axial Strain for All 127.0mm Samples

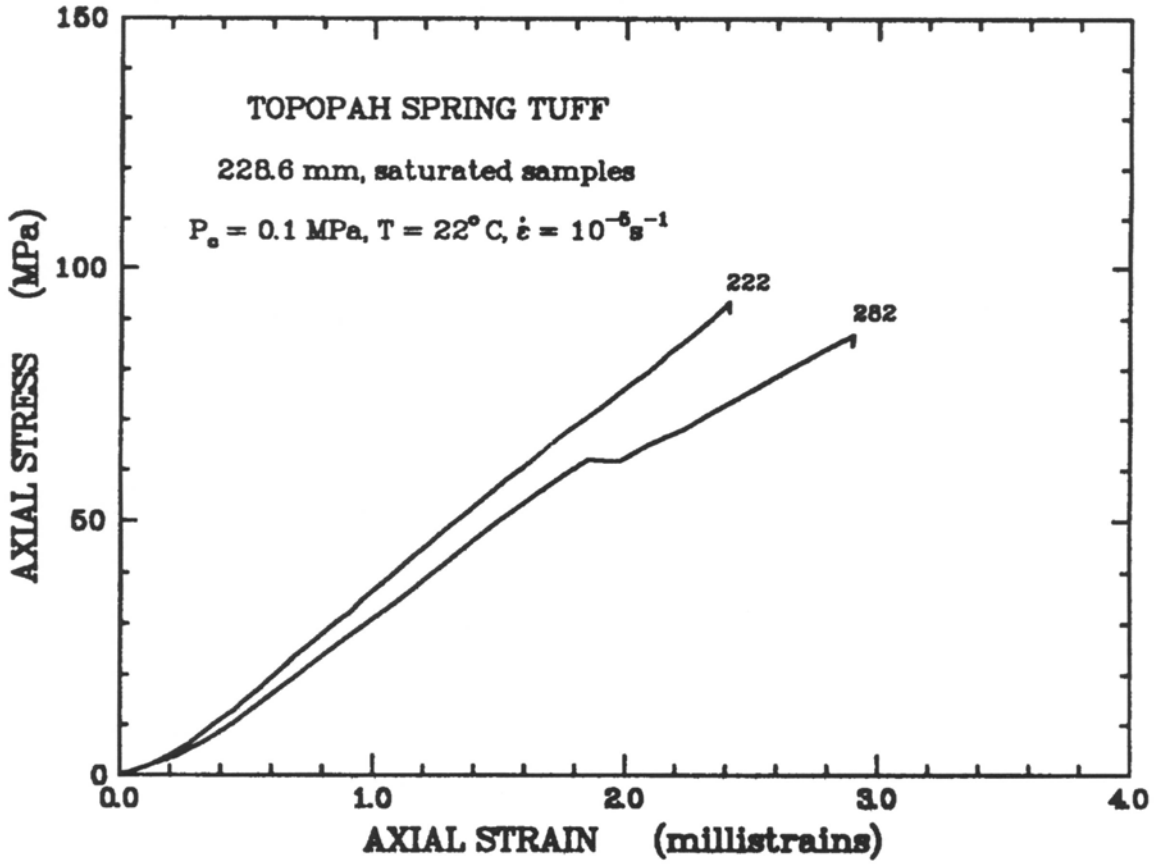

Figure 8.
Plots of Axial Stress Versus Axial Strain for All 228.6mm Samples

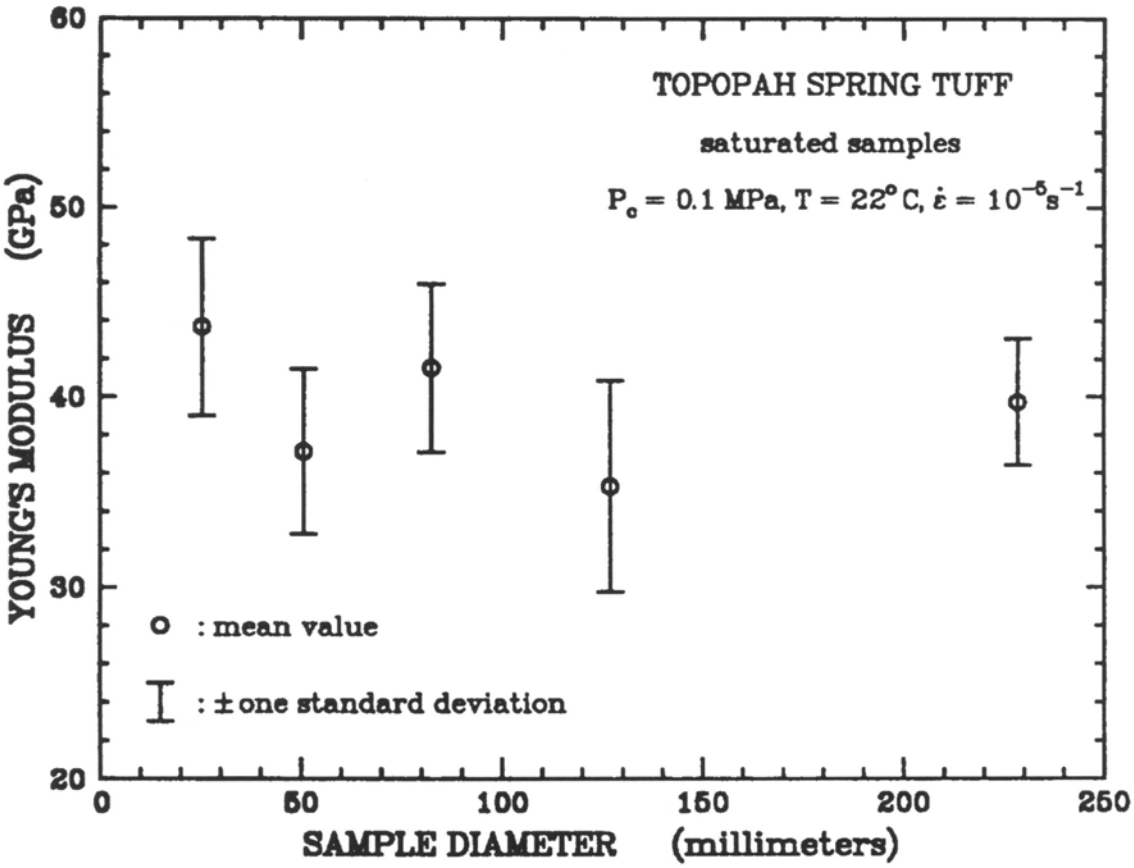

Figure 9.
Plot of Young's Modulus Versus Sample Diameter

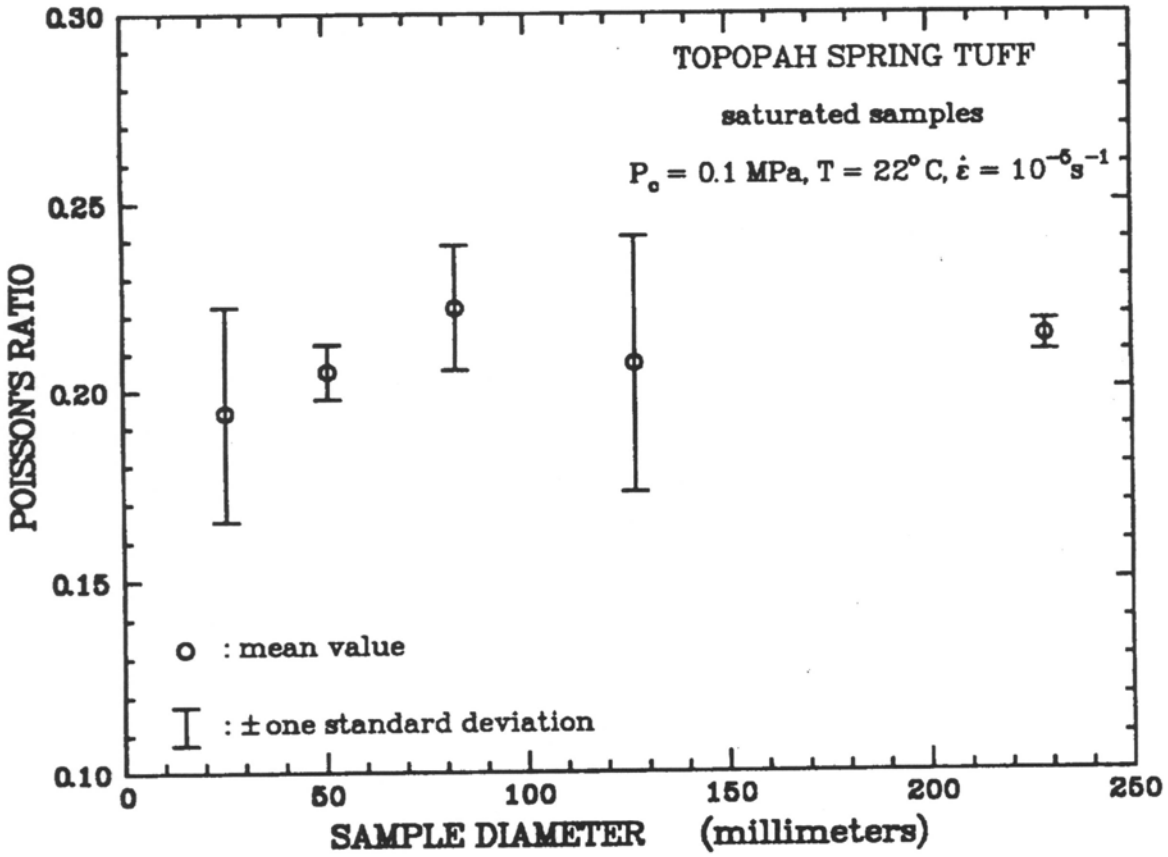

Figure 10.
Plot of Poisson's Ratio Versus Sample Diameter

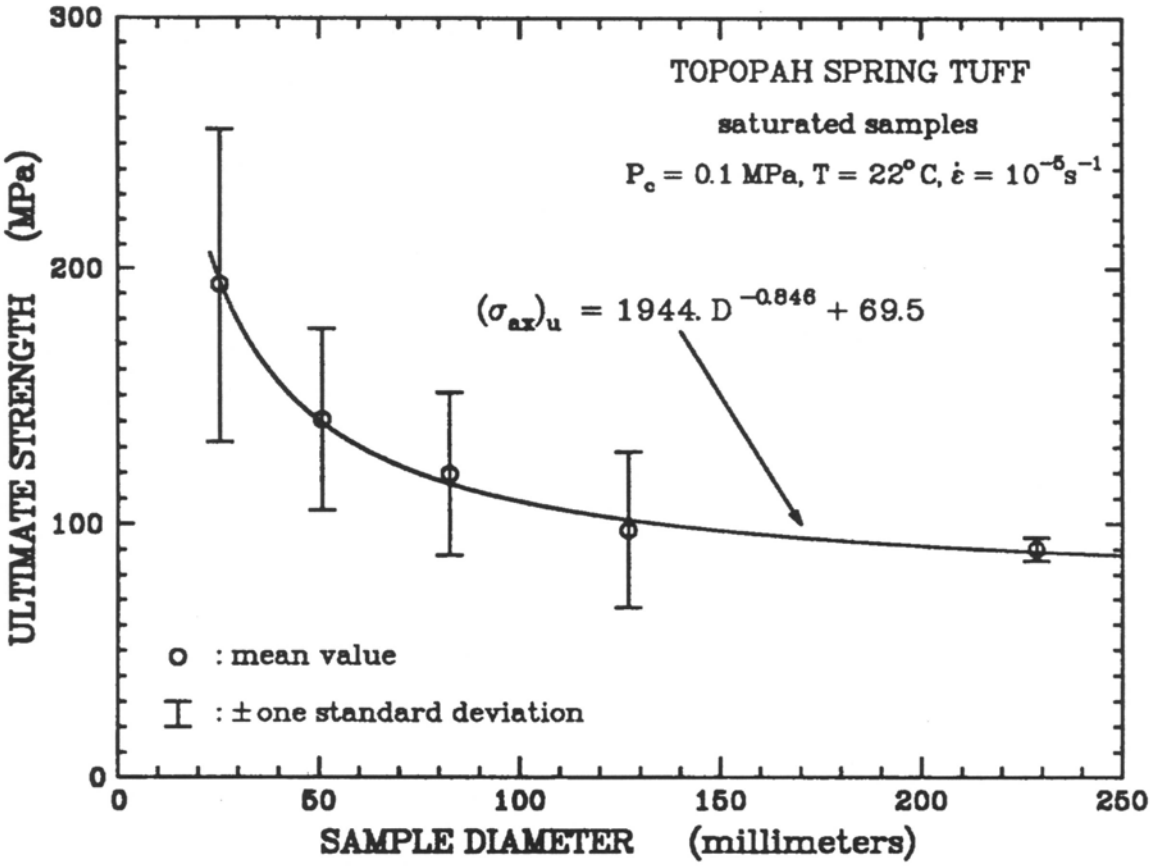

Figure 11.
Plot of Ultimate Strength Versus Sample Diameter

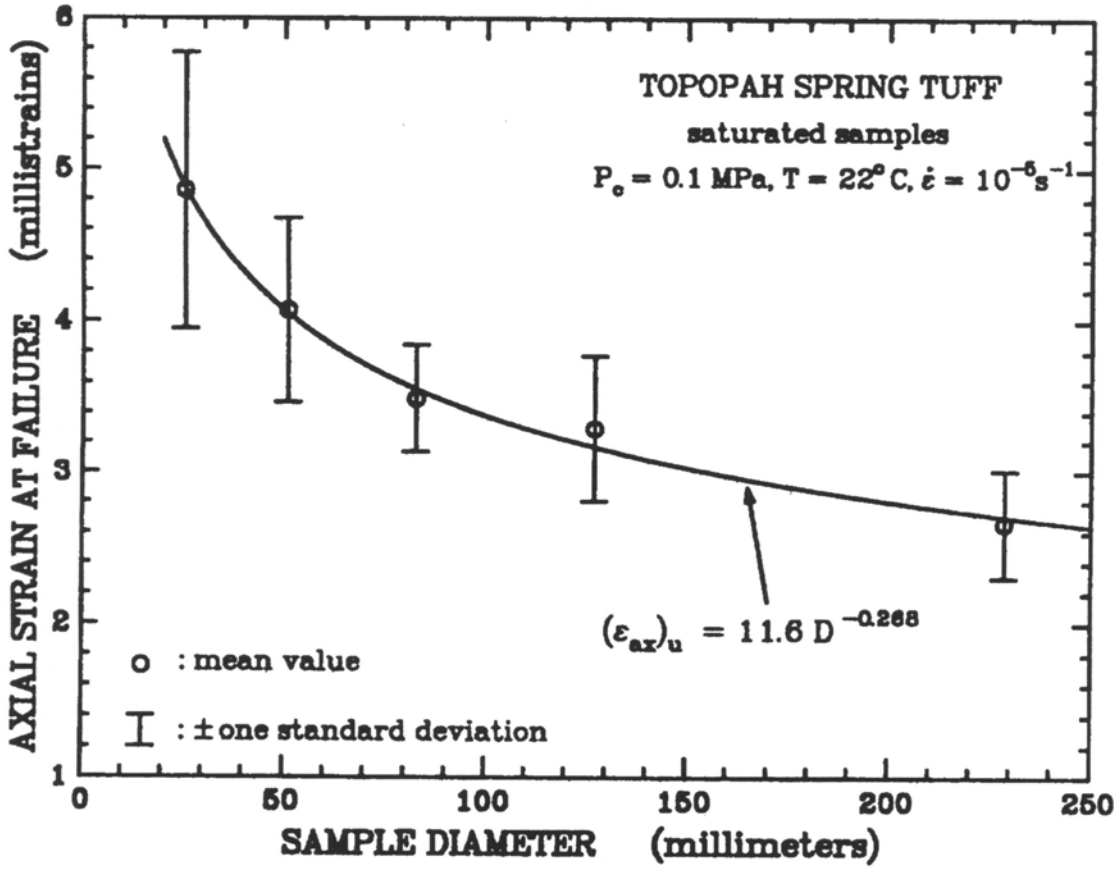

Figure 12.
Plot of Axial Strain at Ultimate Strength Versus Sample Diameter

APPENDIX A.

Calibration Results

As noted in the Experimental Techniques Section (Test Conditions Subsection), the experiments presented in this report were actually run in two major test series, approximately one year apart. During each of the testing sequences, calibrations were run for each subseries of experiments (i.e., each set of tests on a particular sample size).

The test system load cell is calibrated once a year against a standard transducer that is traceable to the U. S. Bureau of Standards (USBS). Before each test series, the axial displacement gages and the transverse displacement gages were calibrated with a calibrator (also traceable to the USBS) described by McNamee (1985). Calibrations of the experimental methods and of the entire instrumentation setup were obtained preceding and following each sub-series by testing an aluminum sample of known mechanical properties. All of these calibration checks were run on 6061-T651 aluminum cylinders (like-sized to the rock samples) with a Young's modulus (E) of 69.7 GPa and a Poisson's ratio (ν) of 0.33. The load cell, axial displacement gage, lateral displacement gage, and system calibration results for each subseries are listed in Tables A-1 through A-5. Table A-6 lists the elastic properties (E and ν) obtained from least-squares fits to the data. The correlation coefficients (R^2) and the percentage errors from the ideal properties (e_m) are also listed.

The axial displacement values for the 82.6 and 127.0 mm diameter samples were taken between the middle of the two steel end-caps. Therefore, the raw displacement measurements also include some of the end-cap deformation. This quantity has been subtracted out; however, since the end-pieces and the sample are two different materials (steel and aluminum), with two different sets of elastic properties, the steel end-caps constrain the ends of the aluminum sample, forcing the lateral deformations (at the ends of the samples) to be less than ideal. Because of these end constraints, the axial displacements are also less than ideal, and as a result, the calculated Young's modulus and Poisson's ratio values are relatively high (see Table A-6). These end effects will be discussed in much more detail by Stavig and Price (in preparation). Axial displacements on the other sized samples were all measured over the middle one-third (approximately) of the sample (both the aluminum and rock samples), with gages mounted directly to the sample.

Table A-1a.
Load Cell, Axial Gage, and Lateral Gage Calibration Data
First Series of 25.4 mm Samples

Load Cell		
f_a (kN)	f_m (kN)	e_m (%)
0.0	0.00	0.0
90.0	89.55	-0.5
180.0	179.37	-0.4
270.0	269.64	-0.1
360.0	360.00	0.0
450.0	450.14	0.0

Axial Gage			Lateral Gage		
δ_a (μm)	δ_m (μm)	e_m (%)	δ_a (μm)	δ_m (μm)	e_m (%)
0.00	0.00	0.0	0.000	0.000	0.0
63.50	63.18	-0.5	5.080	5.156	1.5
127.0	127.8	0.6	10.16	10.45	2.9
190.5	191.1	0.3	15.24	15.49	1.6
254.0	256.0	0.8	20.32	20.51	0.9
317.5	318.5	0.3	25.40	25.53	0.5
381.0	381.6	0.2	30.48	30.84	1.2
444.5	446.3	0.4	35.56	35.78	0.6
508.0	508.3	0.1	40.64	40.85	0.5
571.5	571.8	0.1	45.72	46.01	0.6
635.0	635.3	0.0	50.80	51.00	0.4

Table A-1b.
Aluminum Sample Calibration Data
First Series of 25.4 mm Samples

Pre-Test Series			Post-Test Series		
σ_{ax} (MPa)	ε_{ax} (millistrain)	ε_{lat} (millistrain)	σ_{ax} (MPa)	ε_{ax} (millistrain)	ε_{lat} (millistrain)
0.00	0.000	0.000	0.00	0.000	0.000
6.71	0.083	-0.023	6.86	0.105	-0.027
12.92	0.183	-0.051	13.35	0.215	-0.060
19.49	0.293	-0.081	20.29	0.301	-0.089
25.99	0.392	-0.113	26.54	0.393	-0.118
32.09	0.481	-0.144	33.85	0.496	-0.153
38.74	0.588	-0.174	40.22	0.588	-0.181
45.28	0.671	-0.204	46.99	0.692	-0.213
51.34	0.761	-0.230	53.65	0.792	-0.244
57.85	0.850	-0.262	59.97	0.886	-0.275
64.36	0.945	-0.290	66.41	0.967	-0.301
71.71	1.034	-0.323	74.16	1.084	-0.337
78.28	1.137	-0.356	81.02	1.182	-0.371
84.77	1.222	-0.384	87.13	1.271	-0.398
91.36	1.306	-0.412	93.62	1.352	-0.424

Table A-1c.
Load Cell, Axial Gage, and Lateral Gage Calibration Data
Second Series of 25.4 mm Samples

Load Cell

f_a (kN)	f_m (kN)	e_m (%)
0.0	0.00	0.0
90.0	89.55	-0.5
180.0	179.28	-0.4
270.0	269.55	-0.2
360.0	359.82	-0.1
450.0	449.96	-0.0

Axial Gage			Lateral Gage		
δ_a (μm)	δ_m (μm)	e_m (%)	δ_a (μm)	δ_m (μm)	e_m (%)
0.00	0.00	0.0	0.00	0.00	0.0
25.40	25.35	-0.2	12.70	12.61	-0.7
50.80	50.83	0.1	25.40	25.37	-0.1
76.20	76.38	0.2	38.10	38.09	0.0
101.6	101.8	0.2	50.80	50.81	0.0
127.0	127.0	0.0	63.50	63.63	0.2
152.4	152.5	0.1	76.20	76.56	0.5
177.8	177.6	-0.1	88.90	89.22	0.4
203.2	203.2	0.0	101.6	101.9	0.3
228.6	228.2	-0.2	114.3	114.6	0.3
254.0	254.1	0.0	127.0	127.2	0.2

Table A-1d.
Aluminum Sample Calibration Data
Second Series of 25.4 mm Samples

Pre-Test Series			Post-Test Series		
σ_{ax} (MPa)	ε_{ax} (millistrain)	ε_{lat} (millistrain)	σ_{ax} (MPa)	ε_{ax} (millistrain)	ε_{lat} (millistrain)
0.00	0.000	0.000	0.00	0.000	0.000
9.98	0.148	-0.044	9.39	0.125	-0.040
20.81	0.297	-0.096	19.75	0.267	-0.088
31.27	0.446	-0.144	29.56	0.397	-0.133
40.71	0.580	-0.190	40.09	0.546	-0.185
50.49	0.717	-0.238	50.63	0.693	-0.234
61.20	0.865	-0.289	60.35	0.829	-0.281
70.89	1.000	-0.337	70.05	0.964	-0.326
81.03	1.141	-0.386	80.27	1.109	-0.375
92.25	1.300	-0.441	90.58	1.256	-0.424

Table A-2a.
Load Cell, Axial Gage, and Lateral Gage Calibration Data
First Series of 50.8 mm Samples

Load Cell

f_a (kN)	f_m (kN)	e_m (%)
0.0	0.0	0.0
178.0	180.4	1.3
356.0	358.3	0.6
534.0	535.2	0.2
712.0	712.1	0.0
890.0	888.9	-0.1

Axial Gage

δ_a (mm)	δ_m (mm)	e_m (%)
0.000	0.000	0.0
0.127	0.123	-3.1
0.254	0.249	-2.0
0.381	0.375	-1.6
0.508	0.501	-1.4
0.635	0.627	-1.3
0.762	0.754	-1.0
0.889	0.882	-0.8
1.016	1.011	-0.5
1.143	1.141	-0.2
1.270	1.270	-0.0

Lateral Gage

δ_a (μm)	δ_m (μm)	e_m (%)
0.0	0.0	0.0
76.2	79.3	4.1
127.0	130.7	2.9
177.8	180.5	1.5
228.6	230.4	0.8
279.4	279.7	0.1
317.5	317.5	0.0

Table A-2b.
Aluminum Sample Calibration Data
First Series of 50.8 mm Samples

Pre-Test Series			Post-Test Series*		
σ_{ax} (MPa)	ε_{ax} (millistrain)	ε_{lat} (millistrain)	σ_{ax} (MPa)	ε_{ax} (millistrain)	ε_{lat} (millistrain)
0.000	0.000	0.000			
1.414	0.032	-0.003			
7.630	0.125	-0.034			
16.094	0.231	-0.076			
26.951	0.364	-0.129			
37.331	0.519	-0.178			
46.690	0.650	-0.227			
57.589	0.810	-0.281			
67.205	0.966	-0.330			
78.414	1.131	-0.384			
89.008	1.290	-0.439			
99.716	1.446	-0.492			

* No post-test series calibration check was done.

Table A-2c.
Load Cell, Axial Gage, and Lateral Gage Calibration Data
Second Series of 50.8 mm Samples

Load Cell

f_a (kN)	f_m (kN)	e_m (%)
0.0	0.00	0.0
180.0	180.72	0.4
360.0	360.72	0.2
540.0	540.63	0.1
720.0	720.27	0.0
900.0	900.27	0.0

Axial Gage			Lateral Gage		
δ_a (μm)	δ_m (μm)	e_m (%)	δ_a (μm)	δ_m (μm)	e_m (%)
0.00	0.00	0.0	0.00	0.00	0.0
50.80	50.39	-0.8	31.75	31.91	0.5
101.6	101.0	-0.6	63.50	63.63	0.2
152.4	151.2	-0.8	95.25	95.44	0.2
203.2	201.8	-0.7	127.0	127.0	0.0
254.0	252.4	-0.6	158.8	158.8	0.0
304.8	303.1	-0.6	190.5	190.6	0.1
355.6	353.2	-0.7	222.3	222.4	0.0
406.4	403.9	-0.6	254.0	254.3	0.1
457.2	454.6	-0.6	285.8	285.7	0.0
508.0	505.1	-0.6	317.5	317.9	0.1

Table A-2d.
Aluminum Sample Calibration Data
Second Series of 50.8 mm Samples

Pre-Test Series			Post-Test Series		
σ_{ax} (MPa)	ε_{ax} (millistrain)	ε_{lat} (millistrain)	σ_{ax} (MPa)	ε_{ax} (millistrain)	ε_{lat} (millistrain)
0.00	0.000	0.000	0.00	0.000	0.000
5.79	0.081	-0.026	5.33	0.078	-0.027
11.71	0.167	-0.053	10.89	0.159	-0.055
17.40	0.246	-0.081	16.14	0.238	-0.081
23.14	0.330	-0.108	21.95	0.319	-0.108
27.11	0.387	-0.126	27.71	0.400	-0.136
31.93	0.459	-0.151	33.40	0.481	-0.164
37.31	0.540	-0.176	39.13	0.559	-0.193
43.58	0.630	-0.205	44.69	0.641	-0.219
49.48	0.722	-0.233	50.39	0.721	-0.246
55.16	0.802	-0.261	56.16	0.802	-0.276
61.18	0.889	-0.288	61.78	0.881	-0.303
69.43	1.014	-0.327	67.84	0.970	-0.333
73.64	1.074	-0.348	73.64	1.053	-0.360
78.81	1.150	-0.374	79.08	1.126	-0.388
84.07	1.226	-0.395	85.20	1.210	-0.416
90.29	1.317	-0.428	90.80	1.287	-0.446
93.80	1.369	-0.445	96.67	1.373	-0.474

Table A-3a.
Load Cell, Axial Gage, and Lateral Gage Calibration Data
First Series of 82.6 mm Samples

Load Cell			Axial Gage		
f_a (kN)	f_m (kN)	e_m (%)	δ_a (mm)	δ_m (mm)	e_m (%)
0.0	0.0	0.0	0.0000	0.0000	0.0
178.0	180.4	1.3	0.1270	0.1275	-0.4
356.0	358.3	0.6	0.2540	0.2535	-0.2
534.0	535.2	0.2	0.3810	0.3747	-1.7
712.0	712.1	0.0	0.5080	0.4959	-2.4
890.0	888.9	-0.1	0.6350	0.6185	-2.6
			0.7620	0.7418	-2.7
			0.8890	0.8698	-2.2
			1.016	1.001	-1.5
			1.143	1.134	-0.8
			1.270	1.270	0.0

Lateral Gage 1			Lateral Gage 2		
δ_a (μm)	δ_m (μm)	e_m (%)	δ_a (μm)	δ_m (μm)	e_m (%)
0.00	0.00	0.0	0.00	0.00	0.0
10.16	10.47	3.1	10.16	10.62	4.5
20.32	20.75	2.1	20.32	20.70	1.9
30.48	30.70	0.7	30.48	30.77	1.0
40.64	40.97	0.8	40.64	40.82	0.4
50.80	51.03	0.5	50.80	50.85	0.1
60.96	61.21	0.4	60.96	61.47	0.8
71.12	71.12	0.0	71.12	71.35	0.3
81.28	81.16	-0.1	81.28	81.49	0.3
91.44	91.82	0.4	91.44	91.83	0.4
101.6	101.5	-0.1	101.6	101.8	0.2

Table A-3b.
Aluminum Sample Calibration Data
First Series of 82.6 mm Samples

Pre-Test Series				Post-Test Series			
σ_{az} (MPa)	ε_{az} (millistrain)	ε_{lat1} (milli)	ε_{lat2} (milli)	σ_{az} (MPa)	ε_{az} (millistrain)	ε_{lat1} (milli)	ε^{*}_{lat2}
0.0000	0.0000	0.0000	0.0000	0.0000	0.0000	0.0000	
7.9972	0.1065	-0.0393	-0.0385	6.6398	0.0902	-0.0335	
14.0847	0.1875	-0.0682	-0.0676	12.8790	0.1750	-0.0633	
20.5141	0.2732	-0.1012	-0.0992	19.5207	0.2652	-0.0956	
26.8241	0.3572	-0.1310	-0.1299	25.9218	0.3521	-0.1275	
33.5083	0.4462	-0.1642	-0.1632	32.4361	0.4406	-0.1595	
39.8709	0.5309	-0.1954	-0.1935	39.0313	0.5302	-0.1915	
47.6598	0.6346	-0.2332	-0.2310	45.5740	0.6191	-0.2236	
53.9313	0.7181	-0.2643	-0.2613	52.2704	0.7101	-0.2564	
60.0593	0.7997	-0.2946	-0.2914	59.0032	0.8015	-0.2903	
66.3308	0.8832	-0.3248	-0.3212	65.2040	0.8858	-0.3200	
72.9018	0.9707	-0.3574	-0.3533	71.9226	0.9770	-0.3517	
79.2927	1.0558	-0.3885	-0.3837	78.2894	1.0635	-0.3837	
85.5557	1.1392	-0.4200	-0.4149	84.3564	1.1459	-0.4121	
92.5987	1.2330	-0.4543	-0.4490	91.5784	1.2440	-0.4482	
98.9837	1.3180	-0.4849	-0.4800	97.7854	1.3283	-0.4775	

* The lateral displacement gage was ruined during sample testing.

Table A-3c.
Load Cell, Axial Gage, and Lateral Gage Calibration Data
Second Series of 82.6 mm Samples

Load Cell			Axial Gage		
f_a (kN)	f_m (kN)	e_m (%)	δ_a (mm)	δ_m (mm)	e_m (%)
0.0	0.0	0.0	0.0000	0.0000	0.0
450.0	449.1	-0.2	0.1270	0.1257	-1.0
900.0	895.5	-0.5	0.2540	0.2516	-0.9
1350.0	1346.0	-0.3	0.3810	0.3781	-0.8
1800.0	1793.3	-0.4	0.5080	0.5042	-0.7
2250.0	2243.7	-0.3	0.6350	0.6306	-0.7
			0.7620	0.7570	-0.7
			0.8890	0.8837	-0.6
			1.016	1.011	-0.5
			1.143	1.137	-0.5
			1.270	1.264	-0.5

Lateral Gage 1			Lateral Gage 2		
δ_a (μm)	δ_m (μm)	e_m (%)	δ_a (μm)	δ_m (μm)	e_m (%)
0.00	0.00	0.0	0.00	0.00	0.0
25.40	25.50	0.4	25.40	25.76	1.4
50.80	50.93	0.3	50.80	51.21	0.8
76.20	76.33	0.2	76.20	76.53	0.4
101.6	101.6	0.0	101.6	101.9	0.3
127.0	126.7	-0.2	127.0	127.2	0.2
152.4	152.3	-0.1	152.4	152.5	0.1
177.8	177.8	0.0	177.8	178.1	0.2
203.2	202.7	-0.2	203.2	203.5	0.1
228.6	228.0	-0.3	228.6	229.0	0.2
254.0	253.5	-0.2	254.0	254.4	0.2

Table A-3d.
Aluminum Sample Calibration Data
Second Series of 82.6 mm Samples

Pre-Test Series				Post-Test Series			
σ_{az} (MPa)	ε_{az} (millistrain)	ε_{lat1} (millistrain)	ε_{lat2} (millistrain)	σ_{az} (MPa)	ε_{az} (millistrain)	ε^*_{lat1}	ε^*_{lat2}
0.00	0.000	0.000	0.000	0.00	0.000	-	-
5.05	0.064	-0.024	-0.025	4.93	0.063	-	-
10.04	0.128	-0.049	-0.051	9.68	0.133	-	-
14.81	0.194	-0.072	-0.073	14.34	0.196	-	-
19.53	0.256	-0.093	-0.096	18.86	0.256	-	-
24.48	0.324	-0.117	-0.120	23.48	0.324	-	-
29.41	0.388	-0.140	-0.145	28.65	0.391	-	-
34.39	0.456	-0.165	-0.168	33.74	0.464	-	-
39.44	0.525	-0.190	-0.193	38.75	0.532	-	-
44.40	0.593	-0.214	-0.217	43.81	0.605	-	-
49.07	0.655	-0.236	-0.239	49.05	0.676	-	-
54.21	0.720	-0.259	-0.265	53.71	0.742	-	-
58.78	0.786	-0.282	-0.288	59.04	0.814	-	-
63.88	0.855	-0.307	-0.313	64.18	0.883	-	-
68.54	0.913	-0.328	-0.335	69.49	0.951	-	-
73.80	0.983	-0.354	-0.359	74.07	1.015	-	-
78.77	1.048	-0.378	-0.386	78.93	1.078	-	-
83.99	1.115	-0.403	-0.410	84.17	1.145	-	-
89.22	1.182	-0.428	-0.436	89.67	1.216	-	-
94.32	1.249	-0.453	-0.460	94.26	1.278	-	-
99.68	1.318	-0.478	-0.488	99.21	1.344	-	-

* The lateral displacement gages were ruined during sample testing.

Table A-4a.
Load Cell, Axial Gage, and Lateral Gage Calibration Data
First Series of 127.0 mm Samples

Load Cell			Axial Gage		
f_a (kN)	f_m (kN)	e_m (%)	δ_a (mm)	δ_m (mm)	e_m (%)
0.0	0.0	0.0	0.000	0.000	0.0
445.0	448.8	0.9	1.270	1.198	-5.7
890.0	892.4	0.3	2.540	2.437	-4.1
1335.0	1336.3	0.1	3.810	3.692	-3.1
1780.0	1780.2	0.0	5.080	4.978	-2.0
2225.0	2223.4	-0.1	6.350	6.273	-1.2
			7.620	7.570	-0.7
			8.890	8.871	-0.2
			10.160	10.154	-0.1
			11.430	11.429	0.0
			12.700	12.700	0.0

Lateral Gage 1			Lateral Gage 2		
δ_a (μm)	δ_m (μm)	e_m (%)	δ_a (μm)	δ_m (μm)	e_m (%)
0.00	0.00	0.0	0.00	0.00	0.0
50.80	51.41	1.2	50.80	51.36	1.1
101.60	101.96	0.4	101.60	102.06	0.5
152.40	152.45	0.0	152.40	152.70	0.2
203.20	202.79	-0.2	203.20	203.40	0.1
254.00	253.14	-0.3	254.00	254.05	0.0
304.80	304.09	-0.2	304.80	304.80	0.0
355.60	354.94	-0.2	355.60	355.40	-0.1
406.40	405.94	-0.1	406.40	406.60	0.0
457.20	457.10	0.0	457.20	457.35	0.0
508.00	507.95	0.0	508.00	508.36	0.1

Table A-4b.
Aluminum Sample Calibration Data
First Series of 127.0 mm Samples

Pre-Test Series				Post-Test Series			
σ_{ax} (MPa)	ε_{ax} (millistrain)	ε_{lat1} (milli)	ε_{lat2} (milli)	σ_{ax} (MPa)	ε_{ax} (millistrain)	ε_{lat1} (milli)	ε^{*}_{lat2}
0.0000	0.0000	0.0000	0.0000	0.0000	0.0000	0.0000	
5.0484	0.0671	-0.0244	-0.0256	5.1747	0.0674	-0.0268	
10.3494	0.1375	-0.0495	-0.0491	10.5222	0.1371	-0.0498	
15.6193	0.2076	-0.0740	-0.0734	15.8741	0.2068	-0.0756	
20.8162	0.2766	-0.0980	-0.0990	21.1839	0.2759	-0.1013	
26.0019	0.3456	-0.1211	-0.1209	26.9855	0.3515	-0.1251	
31.3671	0.4169	-0.1486	-0.1459	32.0738	0.4178	-0.1499	
36.5750	0.4861	-0.1693	-0.1713	37.4302	0.4876	-0.1757	
41.8871	0.5567	-0.1982	-0.1954	42.9615	0.5596	-0.2014	
46.9975	0.6246	-0.2195	-0.2209	48.4286	0.6308	-0.2265	
52.3804	0.6961	-0.2481	-0.2437	53.5213	0.6972	-0.2520	
57.6681	0.7664	-0.2715	-0.2719	58.9596	0.7680	-0.2759	
63.1618	0.8394	-0.2975	-0.2958	64.4422	0.8394	-0.3028	
68.2922	0.9076	-0.3206	-0.3212	69.9736	0.9115	-0.3270	
73.6529	0.9788	-0.3472	-0.3466	75.1172	0.9785	-0.3500	
78.7590	1.0467	-0.3693	-0.3702	80.6512	1.0506	-0.3786	
83.7810	1.1134	-0.3939	-0.3934	86.0602	1.1210	-0.4037	
88.8340	1.1806	-0.4175	-0.4163	91.6162	1.1934	-0.4293	
94.1720	1.2515	-0.4445	-0.4414				
99.1870	1.3181	-0.4674	-0.4649				

* The lateral displacement gage was ruined during sample testing.

Table A-4c.
Load Cell, Axial Gage, and Lateral Gage Calibration Data
Second Series of 127.0 mm Samples

Load Cell

f_a (MN)	f_m (MN)	e_m (%)
0.000	0.0000	0.0
0.450	0.4491	-0.2
0.900	0.8955	-0.5
1.350	1.3460	-0.3
1.800	1.7933	-0.4
2.250	2.2437	-0.3

Axial Gage

δ_a (mm)	δ_m (mm)	e_m (%)
0.0000	0.0000	0.0
0.3175	0.3172	-0.1
0.6350	0.6337	-0.2
0.9525	0.9506	-0.2
1.2700	1.2690	-0.1
1.5875	1.5869	-0.0
1.9050	1.9056	0.0
2.2225	2.2228	0.0
2.5400	2.5406	0.0

Lateral Gage

δ_a (mm)	δ_m (mm)	e_m (%)
0.0000	0.0000	0.0
0.1270	0.1271	0.1
0.2540	0.2545	0.2
0.3810	0.3816	0.2
0.5080	0.5089	0.2
0.6350	0.6358	0.1
0.7620	0.7628	0.1
0.8890	0.8895	0.1
1.0160	1.0163	0.0
1.1430	1.1429	0.0
1.2700	1.2696	0.0

Table A-4d.
Aluminum Sample Calibration Data
Second Series of 127.0 mm Samples

Pre-Test Series			Post-Test Series		
σ_{az} (MPa)	ε_{az} (millistrain)	ε_{lat} (millistrain)	σ_{az} (MPa)	ε_{az} (millistrain)	ε_{lat} (millistrain)
0.0000	0.0000	0.0000	0.0000	0.0000	0.0000
7.9237	0.1008	-0.0314	9.1334	0.1279	-0.0461
15.9392	0.2157	-0.0725	19.0158	0.2655	-0.0909
24.4711	0.3186	-0.1145	28.7819	0.3886	-0.1303
33.0166	0.4422	-0.1576	38.4988	0.5094	-0.1881
41.4144	0.5580	-0.2028	48.6875	0.6516	-0.2304
50.1073	0.6713	-0.2348	58.8583	0.7802	-0.2723
58.7174	0.7853	-0.2799	68.4188	0.9190	-0.3301
67.4148	0.8950	-0.3235	78.1782	1.0388	-0.3729
76.1770	1.0237	-0.3703	88.7224	1.1694	-0.4178
85.0957	1.1266	-0.4081	98.5864	1.3061	-0.4661
94.0418	1.2519	-0.4513			

Table A-5a.
Load Cell, Axial Gage, and Lateral Gage Calibration Data
Second Series of 228.6 mm Samples

Load Cell

f_a (MN)	f_m (MN)	e_m (%)
0.000	0.000	0.0
0.900	0.900	0.0
1.800	1.799	-0.1
2.250	2.247	-0.1

Axial Gage			Lateral Gage		
δ_a (mm)	δ_m (mm)	e_m (%)	δ_a (μm)	δ_m (μm)	e_m (%)
0.000	0.0000	0.0	0.00	0.00	0.0
0.127	0.1273	0.2	50.80	50.39	-0.8
0.254	0.2543	0.1	101.6	101.0	-0.6
0.381	0.3810	0.0	152.4	151.2	-0.8
0.508	0.5079	0.0	203.2	201.8	-0.7
0.635	0.6347	0.0	254.0	252.4	-0.6
0.762	0.7617	0.0	304.8	303.1	-0.6
0.889	0.8886	0.0	355.6	353.2	-0.7
1.016	1.0159	0.0	406.4	403.9	-0.6
1.143	1.1434	0.0	457.2	454.6	-0.6
1.270	1.2708	0.0	508.0	505.1	-0.6

Table A-5b.
Aluminum Sample Calibration Data
Second Series of 228.6 mm Samples

Pre-Test Series			Post-Test Series		
σ_{ax} (MPa)	ε_{ax} (millistrain)	ε_{lat} (millistrain)	σ_{ax} (MPa)	ε_{ax} (millistrain)	ε_{lat} (millistrain)
0.00	0.000	0.000	0.00	0.000	0.000
4.53	0.057	-0.021	4.30	0.055	-0.021
9.11	0.131	-0.041	8.81	0.125	-0.042
13.39	0.186	-0.060	13.16	0.185	-0.059
17.71	0.244	-0.081	17.87	0.249	-0.081
22.38	0.320	-0.102	22.43	0.320	-0.102
26.80	0.376	-0.120	26.84	0.379	-0.121
31.45	0.446	-0.143	31.09	0.441	-0.139
35.52	0.506	-0.162	35.43	0.501	-0.161
39.85	0.565	-0.182	39.80	0.565	-0.181
44.28	0.628	-0.200	44.18	0.625	-0.200
48.65	0.694	-0.221	48.47	0.693	-0.217
53.34	0.758	-0.242	53.17	0.763	-0.241
57.39	0.817	-0.262	57.48	0.819	-0.261
61.77	0.877	-0.281	61.54	0.880	-0.279
66.50	0.948	-0.302	66.21	0.945	-0.299
70.79	1.008	-0.321	70.90	1.009	-0.321
75.39	1.078	-0.344	75.59	1.074	-0.340
80.07	1.144	-0.368	80.11	1.146	-0.362
84.40	1.203	-0.384	84.69	1.210	-0.384
88.99	1.271	-0.405	89.38	1.278	-0.406
93.52	1.329	-0.424	93.82	1.344	-0.425

Table A-6.
Young's Modulus and Poisson's Ratio Data from Aluminum Calibration Checks

Diameter (mm)	pre/post-Series	E (GPa)	R^2	e_m (%)	ν	R^2	e_m (%)
25.4	pre-1	69.32	0.999	-0.5	0.318	0.999	-3.6
25.4	post-1	69.13	1.000	-0.8	0.317	1.000	-3.9
25.4	pre-2	71.20	1.000	2.2	0.342	1.000	3.6
25.4	post-2	72.04	1.000	3.4	0.339	1.000	2.7
50.8	pre-1	69.34	0.999	-0.5	0.344	0.999	4.2
50.8	pre-2	68.24	1.000	-2.1	0.324	1.000	-1.8
50.8	post-2	70.60	1.000	1.3	0.345	1.000	4.5
82.6	pre-1	75.10	1.000	†	0.366*	1.000	†
82.6	post-1	73.62	1.000	†	0.360	1.000	†
82.6	pre-2	75.19	1.000	†	0.364*	1.000	†
82.6	post-2	73.53	1.000	†	‡	‡	‡
127.0	pre-1	75.25	1.000	†	0.353*	1.000	†
127.0	post-1	76.77	1.000	†	0.359	1.000	†
127.0	pre-2	74.99	1.000	†	0.364	1.000	†
127.0	post-2	75.85	1.000	†	0.359	1.000	†
228.6	pre-2	69.91	1.000	0.3	0.319	1.000	-3.3
228.6	post-2	69.76	1.000	0.1	0.315	1.000	-4.5

* These data are the average of two measurements.
† These values were not calculated because of sample end effects (see text for discussion).
‡ The lateral displacement gage was destroyed during testing of the rock samples.

APPENDIX B.

The following portions of this document are candidate information for the NNWSI Reference Information Base (RIB):

Equations 1 and 2.

The following portions of this document are candidate information for the NNWSI Tuff Data Base (TDB):

Tables 3 and 4.

DISTRIBUTION LIST

B. C. Rusche, Director (RW-1)
Office of Civilian Radioactive
Waste Management
U. S. Department of Energy
Forrestal Building
Washington, D. C. 20585

R. Stein (RW-24)
Office of Geologic Repositories
U. S. Department of Energy
Forrestal Building
Washington, D. C. 20585

J. J. Fiore (RW-22)
Program Management Division
Office of Geologic Repositories
U. S. Department of Energy
Forrestal Building
Washington, D. C. 20585

M. W. Frei (RW-24)
Engineering & Licensing Division
Office of Geologic Repositories
U. S. Department of Energy
Forrestal Building
Washington, D. C. 20585

E. S. Burton (RW-25)
Siting Division
Office of Geologic Repositories
U. S. Department of Energy
Forrestal Building
Washington, D. C. 20585

C. R. Cooley (RW-24)
Geosciences & Technology Division
Office of Geologic Repositories
U. S. Department of Energy
Forrestal Building
Washington, D. C. 20585

V. J. Cassella (RW-22)
Office of Geologic Repositories
U. S. Department of Energy
Forrestal Building
Washington, D. C. 20585

T. P. Longo (RW-25)
Program Management Division
Office of Geologic Repositories
U. S. Department of Energy
Forrestal Building
Washington, D. C. 20585

C. Klingsberg (RW-24)
Geosciences & Technology Division
Office of Geologic Repositories
U. S. Department of Energy
Forrestal Building
Washington, D. C. 20585

B. G. Gale (RW-25)
Siting Division
Office of Geologic Repositories
U. S. Department of Energy
Forrestal Building
Washington, D. C. 20585

R. J. Blaney (RW-22)
Program Management Division
Office of Geologic Repositories
U. S. Department of Energy
Forrestal Building
Washington, D. C. 20585

R. W. Gale (RW-40)
Office of Policy, Integration, and
and Outreach
U. S. Department of Energy
Forrestal Building
Washington, D. C. 20585

J. E. Shaheen (RW-44)
Outreach Programs
Office of Policy, Integration,
and Outreach
U. S. Department of Energy
Forrestal Building
Washington, D. C. 20585

J. O. Neff
Salt Repository Project Office
U. S. Department of Energy
505 King Avenue
Columbus, OH 43201

D. C. Newton (RW-23)
Engineering & Licensing Division
Office of Geologic Repositories
U. S. Department of Energy
Forrestal Building
Washington, D. C. 20585

O. L. Olson, Manager
Basalt Waste Isolation Project Office
U. S. Department of Energy
Richland Operations Office
Post Office Box 550
Richland, WA 99352

D. L. Vieth, Director (4)
Waste Management Project Office
U. S. Department of Energy
Post Office Box 14100
Las Vegas, NV 89114

D. F. Miller, Director
Office of Public Affairs
U. S. Department of Energy
Post Office Box 14100
Las Vegas, NV 89114

P. M. Bodin (12)
Office of Public Affairs
U. S. Department of Energy
Post Office Box 14100
Las Vegas, NV 89114

B. W. Church, Director
Health Physics Division
U. S. Department of Energy
Post Office Box 14100
Las Vegas, NV 89114

Chief, Repository Projects Branch
Division of Waste Management
U. S. Nuclear Regulatory Commission
Washington, DC 20555

Document Control Center
Division of Waste Management
U. S. Nuclear Regulatory Commission
Washington, DC 20555

S. A. Mann, Manager
Crystalline Rock Project Office
U. S. Department of Energy
9800 South Cass Avenue
Argonne, IL 60439

K. Street, Jr.
Lawrence Livermore National Laboratory
Post Office Box 808
Mail Stop L-209
Livermore, CA 94550

L. D. Ramspott (3)
Technical Project Officer for NNWSI
Lawrence Livermore National Laboratory
Post Office Box 808
Mail Stop L-204
Livermore, CA 94550

W. J. Purcell (RW-20)
Office of Geologic Repositories
U. S. Department of Energy
Forrestal Building
Washington, D. C. 20585

D. T. Oakley (4)
Technical Project Officer for NNWSI
Los Alamos National Laboratory
Post Office Box 1663
Mail Stop F-619
Los Alamos, NM 87545

W. W. Dudley, Jr. (3)
Technical Project Officer for NNWSI
U. S. Geological Survey
Post Office Box 25046
418 Federal Center
Denver, CO 80225

NTS Section Leader
Repository Projects Branch
Division of Waste Management
U. S. Nuclear Regulatory Commission
Washington, DC 20555

V. M. Glanzman
U. S. Geological Survey
Post Office Box 25046
913 Federal Center
Denver, CO 80225

P. T. Prestholt
NRC Site Representative
1050 East Flamingo Road
Suite 319
Las Vegas, NV 89109

M. E. Spaeth
Technical Project Officer for NNWSI
Science Applications International, Corp.
2769 South Highland Drive
Las Vegas, NV 89109

SAIC-T&MSS Library (2)
Science Applications International, Corp.
2950 South Highland Drive
Las Vegas, NV 89109

W. S. Twenhofel, Consultant
Science Applications International, Corp.
820 Estes Street
Lakewood, CO 80215

A. E. Gurrola, General Manager
Energy Support Division
Holmes & Narver, Inc.
Post Office Box 14340
Las Vegas, NV 89114

J. A. Cross, Manager
Las Vegas Branch
Fenix & Scisson, Inc.
Post Office Box 15408
Las Vegas, NV 89114

N. Duncan (RW-44)
Office of Policy, Integration,
and Outreach
U. S. Department of Energy
Forrestal Building
Washington, D. C. 20585

J. Fordham
Desert Research Institute
Water Resources Center
Post Office Box 60220
Reno, NV 89506

J. S. Wright
Technical Project Officer for NNWSI
Westinghouse Electric Corporation
Waste Technology Services Division
Nevada Operations
Post Office Box 708
Mail Stop 703
Mercury, NV 89023

ONWI Library
Battelle Columbus Laboratory
Office of Nuclear Waste Isolation
505 King Avenue
Columbus, OH 43201

W. M. Hewitt, Program Manager
Roy F. Weston, Inc.
2301 Research Blvd., 3rd. Floor
Rockville, MD 20850

H. D. Cunningham, General Manager
Reynolds Electrical & Engineering Company, Inc.
Post Office Box 14400
Mail Stop 555
Las Vegas, NV 89114

T. Hay, Executive Assistant
Office of the Governor
State of Nevada
Capitol Complex
Carson City, NV 89710

R. R. Loux, Jr., Director (3)
Nuclear Waste Project Office
State of Nevada
Capitol Complex
Carson City, NV 89710

C. H. Johnson, Technical
Program Manager
Nuclear Waste Project Office
State of Nevada
Capitol Complex
Carson City, NV 89710

Dr. M. Mifflin
Desert Research Institute
Water Resources Center
Suite 1
2505 Chandler Avenue
Las Vegas, NV 89120

Department of Comprehensive Planning
Clark County
225 Bridger Avenue, 7^{th} Floor
Las Vegas, NV 89155

Lincoln County Commission
Lincoln County
Post Office Box 90
Pioche, NV 89043

Community Planning and Development
City of North Las Vegas
Post Office Box 4086
North Las Vegas, NV 89030

City Manager
City of Henderson
Henderson, NV 89015

N. A. Norman
Project Manager
Bechtel National Inc.
Post Office Box 3965
San Francisco, CA 94119

F. Butler
Los Alamos Technical Associates
1650 Trinity Drive
Los Alamos, NM 87544

T. G. Barbour
Science Applications
International Corporation
1626 Cole Boulevard, Suite 270
Golden, CO 80401

Planning Department
Nye County
Post Office Box 153
Tonopah, NV 89049

Economic Development Department
City of Las Vegas
400 East Stewart Avenue
Las Vegas, NV 89101

Director of Community Planning
City of Boulder City
Post Office Box 367
Boulder City, NV 89005

Commission of European Communities
200 Rue de la Loi
B-1049 Brussels
BELGIUM

Technical Information Center
Roy F. Weston, Inc.
2301 Research Boulevard,
Third Floor
Rockville, MD 20850

R. Harig
Parsons, Brinkerhoff, Quade, &
Douglass, Inc.
1625 Van Ness Avenue
San Francisco, CA 94109-3678

Dr. M. M. Singh, President
Engineers International, Inc.
98 East Naperville Road
Westmont, IL 60559-1595

Dr. N. L. Carter, Director
Center for Tectonophysics
Texas A& M University
College Station, TX 77843

RE/SPEC, Inc. (2)
Post Office Box 725
Rapid City, SD 57701
Attention:
P. F. Gnirk
P. E. Senseny

RE/SPEC, Inc. (2)
Post Office Box 14984
Albuquerque, NM 87191
Attention:
S. W. Key
D. K. Parrish

R. Coppage, Senior Mining Engineer
Fenix & Scisson, Inc.
Post Office Box 498
Mercury, NV 89023

Christopher Barton
U. S. Geological Survey
Post Office Box 327
Mercury, NV 89023

Eugene P. Binnall
Field Systems Group
Building 50B/4235
Lawrence Berkeley Laboratory
University of California
Berkeley, CA 94720

J. D. Blacic
Los Alamos National Laboratory
Post Office Box 1663
Mail Stop J-980
Los Alamos, NM 87545

R. E. Riecker
Los Alamos National Laboratory
Post Office Box 1663
Group ESS-3
Los Alamos, NM 87545

R. Newmark
Lawrence Livermore National Laboratory
Post Office Box 808
Mail Stop L-221
Livermore, CA 94550

T. H. Isaacs (RW-22)
Office of Geologic Repositories
U. S. Department of Energy
Forrestal Building
Washington, D. C. 20585

D. H. Alexander (RW-24)
Office of Geologic Repositories
U. S. Department of Energy
Forrestal Building
Washington, D. C. 20585

J. P. Knight (RW-23)
Office of Geologic Repositories
U. S. Department of Energy
Forrestal Building
Washington, D. C. 20585

A. Jelacic (RW-24)
Office of Geologic Repositories
U. S. Department of Energy
Forrestal Building
Washington, D. C. 20585

G. Parker (RW-25)
Office of Geologic Repositories
U. S. Department of Energy
Forrestal Building
Washington, D. C. 20585

J. R. Rollo
Deputy Assistant Director
for Engineering Geology
U. S. Geological Survey
106 National Center
12201 Sunrise Valley Drive
Reston, VA 22092

B. J. King, Librarian
Basalt Waste Isolation Project Library
Rockwell Hanford Operations
Post Office Box 800
Richland, WA 99352

C. M. St. John
J. F. T. Agapito Associates, Inc.
27520 Hawthorne Blvd., Suite 137
Rolling Hills Estates, CA 90274

Roger Hart
Itasca Consulting Group, Inc.
Post Office Box 14806
Minneapolis, MN 55414

1510 J. W. Nunziato
1520 D. J. McCloskey
1521 R. D. Krieg
1524 A. K. Miller
1524 K. W. Schuler
1530 L. W. Davison
1534 J. R. Asay
1540 W. C. Luth
1541 H. C. Hardee
1542 W. H. Gerstle
1542 D. J. Holcomb
1542 W. A. Olsson
1542 R. H. Price (20)
1542 L. W. Teufel
1542 W. R. Wawersik
1543 T. M. Gerlach
3141 S. A. Landenberger (5)
3151 W. L. Garner (3)
3154-1 C. H. Dalin, for DOE/OSTI (28)
6300 R. W. Lynch
6310 T. O. Hunter
6310 51/L02A1.A-02/24/84
6310 51/L02A1.A-06/26/85
6311 C. Mora (2)
6311 L. W. Scully
6312 F. W. Bingham
6312 B. S. Langkopf
6313 T. E. Blejwas
6313 F. B. Nimick (4)
6313 B. M. Schwartz
6313 A. Stevens
6313 R. M. Zimmerman
6314 S. J. Bauer
6314 L. S. Costin
6314 B. L. Ehgartner
6314 A. J. Mansure
6314 J. R. Tillerson
6315 M. J. Eatough
6315 S. Sinnock
6315 D. H. Zeuch (2)
6332 WMT Library (20)
6430 N. R. Ortiz
7417 F. L. McFarling
8024 P. W. Dean